Hindawi
Mathematical Problems in Engineering
Volume 2022, Article ID 2812671, 22 pages
https://doi.org/10.1155/2022/2812671

Research Article

Design of a Fixed-Wing UAV Controller Combined Fuzzy Adaptive Method and Sliding Mode Control

Yufei Guo,[1] **Leru Luo**,[2] **and Changchun Bao**[3]

[1]*School of Electrical Engineering, University of New South Wales, Kensington, Australia*
[2]*Department of Theoretical Mechanics, Inner Mongolia University of Technology, Hohhot, China*
[3]*Department of Aviation Engineering, Inner Mongolia University of Technology, Hohhot, China*

Correspondence should be addressed to Changchun Bao; imut007@163.com

Received 23 October 2021; Accepted 22 December 2021; Published 31 January 2022

Academic Editor: Francisco Rossomando

To overcome the complexity of the coupled nonlinear model of a fixed-wing UAV system and the uncertainty caused by a large number of interference factors, a control algorithm combining fuzzy adaptive control and sliding mode variable structure control was proposed. The controller algorithm mainly relies on the sliding mode variable structure control method to solve the control problem of the strongly coupled complex nonlinear system. Based on sliding mode control, a fuzzy adaptive method is introduced to reduce the chattering problem of the traditional sliding mode control, and the uncertain parameters and unknown functions caused by external disturbances are approximated by this method. In this study, two types of fuzzy adaptive sliding mode controller were designed according to the different object ranges of the fuzzy adaptive algorithm. In addition, the stability of the controllers was verified using the Lyapunov method. Finally, numerical simulations are performed to demonstrate the effectiveness of the proposed controllers by comparing with the traditional sliding mode controller.

1. Introduction

Recently, unmanned aerial vehicles (UAVs) have been widely utilized in military and civil applications. The mainstream UAV types are four-rotor, six-rotor, cross-double-rotor, helicopter, and fixed-wing UAV. They are applied to different fields based on their characteristics. Fixed-wing UAVs are always used to complete tasks requiring high speed and altitude according to their characteristics: fast flying speed, high flying altitude, and flexible attitude [1]. The biggest problem with fixed-wing UAV control is related to its complex model. This is mainly because this type of UAV model is multiple-state variables deeply coupled, nonlinear, and multiple interference factors. Therefore, accurate modeling is a difficult and tedious task.

A large number of studies have been conducted on the model establishment of fixed-wing UAVs, but they can only provide models closed to the real situation [2–4]. To compensate for the inaccuracy of the model, many robust control algorithms have been applied to fixed-wing UAV controllers. In this field, a number of feasible control algorithms have been proposed, including neural control [5], linear tracking control [6], robust nonlinear control [7–9], adaptive output-feedback tracking control [10–12], multi-objective control [13], dynamic gain scheduling control [14], slide mode control [13, 15], and fuzzy control [15].

Gomez et al. (2011) suggested utilizing a combination of fuzzy logic control and model reference adaptive control to stabilize and control a fixed-wing UAV [15]. The feasibility and robustness of this algorithm were verified through relevant simulations. Zhou et al. combined the linear feedback control method and adaptive control method to design a controller based on the attitude angle of a fixed-wing UAV in 2014 [16]. The adaptive control law is derived using MRC theory. Experiments have proved the superior performance of this controller compared with a traditional PID controller. Espinoza et al. designed five different nonlinear controllers for a fixed-wing UAV to compare their performances in 2014 [17]. These controllers were the backstepping controller, sliding mode controller,

backstepping sliding mode controller, backstepping second-order sliding mode controller, and backstepping high-order sliding mode controller. Open-loop experiments verified that the backstepping high-order sliding mode controller could eliminate the shaking phenomenon effectively and completely. Poksawat and his team also proposed an automatic tuning control method for the attitude system of a fixed-wing UAV in 2016 [18]. This method identified the open-loop frequency response of the system through a closed-loop relay feedback experiment and identified the time-delayed accretor model of the inner and outer rings to calculate the control parameters according to the specified gain and phase margin. The reliability of this method was verified through wind tunnel experiments. Zheng et al. (2017) proposed an adaptive sliding mode control law that allows a fixed-wing UAV to track the desired landing path while keeping the pitch angle and roll angle unchanged [19]. The experimental results showed that the proposed control algorithm can suppress the shaking. Castañeda and his partners (2017) claimed that an extended observer based on the adaptive second-order sliding mode control method they designed could help to control the attitude of a fixed-wing UAV smoothly [20]. The main function of the observer was to identify and estimate unknown disturbance bounds to ensure the stability of the system. The simulation results showed that the observer had a good tracking performance for unknown disturbances. Melkou et al. introduced a second-order sliding mode control method to achieve the attitude control process of a fixed-wing UAV in 2018 [21]. The shaking problem was solved using second-order sliding mode control. The uncertainty of the model interference was compensated by introducing an adaptive law. Experiments showed that this method can stably and effectively control the attitude angle. Li et al. (2018) attempted to use a synthetic jet actuator (SJAs) to achieve thrust vector control of a fixed-wing UAV [22]. The pitching attitude controller was designed by combining this novel control method with sliding mode control, and the practicability of the controller was proved by relevant experiments. Also, in 2018, a gain-scheduled proportional integral derivative control system for a fixed-wing UAV was proposed by Poksawat [23]. This controller utilizes an automatic tuning algorithm to adjust the control parameters to achieve an adaptive process. The experimental results showed that this controller is feasible for improving the performance of a traditional linear control system. Zhang et al. presented a multivariable finite-time observer-based adaptive gain sliding mode control scheme for a fixed-wing UAV subject to unmeasurable angular rates and unknown matched/unmatched disturbance in 2021 [24]. They constructed a multivariable finite-time observer to estimate the unknown state of the attitude control system. Experiments showed that the observer could estimate the uncertainty of the system effectively. In 2021, Jun et al. explored the output-feedback control (OFC) strategy design problem for a type of the Takagi-Sugeno fuzzy singular perturbed system [25]. They proposed a novel stochastic communication protocol (SCP) to alleviate the communication load and improve the reliability of signal transmission. The validity of the attained methodology was expressed through a practical example. Yueying Wang and his team proposed an integral sliding mode control strategy for a kind of Takagi-Sugeno fuzzy approximation-based nonlinear SPDSs under time-varying nonlinear perturbation in 2020 [26]. In this study, the sliding mode dynamics (SMD) is transformed into an augmented form to facilitate the synthesis of the high-level controller (HLC). The applicability of the developed FISMC strategy was testified by a practical example. Qi et al. (2020) introduced an appropriate fuzzy SMC law under the complex stochastic semi-Markovian switching process [27]. Compared with previous literature, novel integral sliding mode surfaces (ISMSs) were developed to depend on the designed controller gains and projection matrices in this study. The effectiveness of the theoretical findings was illustrated through an electric circuit model illustrates.

According to existing research, for this type of complex nonlinear model, sliding mode control is a more popular control method. Therefore, the sliding mode control method is also utilized as basic control mean to design the relevant controller to overcome the control problem of the complex nonlinear system. However, there are two main problems to overcome when using the sliding mode control method to control fixed-wing UAVs.

The first problem is how to deal with the effects of unknown external disturbances on the system. Owing to the complexity of the fixed-wing UAV model, there are many relevant unknown disturbances that affect the stability of the system. At present, the main way to cancel interference is to introduce an observer to predict interference. A disturbance observer can observe internal disturbances well and provide compensation for the system; however, its effect on external disturbances is not obvious. The design in this study adopts a combination with the adaptive method and fuzzy method to deal with the impact of internal and external disturbances simultaneously. The fuzzy model used in this study is the T-S fuzzy model. T-S fuzzy model is composed of multiple linear systems fitting the same nonlinear system, using the fuzzy algorithm to deconstruct the input variables, and then defuzzifying through fuzzy calculus reasoning, generating several equations representing the relationship between the input and output of each group [25, 27, 28]. This model was proposed by Takagi and Sugeno in 1985. At present, it has become the most popular fuzzy model in many fuzzy control algorithm designs. In this study, five membership functions are used as the relationship between fuzzy input and fuzzy output to deconstruct the changes of $F(x)$ and $G(x)$, and they are divided into five sections by if-then principle, respectively. At the same time, according to the fuzzy approximation theory, the fuzzy system with an adaptive law can make the approximation error very small by adaptive parameters, which means that appropriate adaptive parameters can help the adaptive fuzzy sliding mode control system to reach the sliding mode surface gradually and stably. It is the reason of the introduction of an adaptive law. Consequently, this method is introduced to approximate the model of fixed-wing UAV basic on sliding mode control. In this way, the influence of internal uncertainty and external interference on the system of fixed-wing UAV can be overcome.

The second problem is how to deal with the shaking. The shaking problem is a common phenomenon associated with the sliding mode control. The problem of shaking is mainly caused by the phenomenon that when the controlled system approaches the sliding mode surface under the action of the control law, it cannot stay on the sliding mode surface perfectly and vibrates around the sliding mode surface many times. From the references mentioned above, it can be seen that many scholars are currently working on how to overcome shaking. Most of them attempted to introduce an adaptive method, a second-order sliding mode method, or a high-order sliding mode method to fix this problem. In this study, a new method is proposed that to adopt a fuzzy method to overcome the shaking in a sliding mode controller. Utilizing the same adaptive fuzzy method above to eliminate shaking by the fuzzy processing of the switching item is also the key point of this study. Three membership functions are taken as relationship between fuzzy input and fuzzy output to deconstruct the switching term' change and divide it into three sections by if-then principle. Similarly, an adaptive method and T-S fuzzy model are combined to achieve fuzzy approximation of the switching term to solve the chattering problem.

At present, there are few studies on the use of fuzzy methods to eliminate shaking. The innovation of this study is to combine the fuzzy method, sliding mode control, and adaptive method to overcome shaking and uncertainty interference.

According to this, two different types of controllers are designed in this study. The first is a fuzzy adaptive sliding mode controller for switching terms only. The controller is mainly used to solve the chattering problem caused by sliding mode control and can overcome part of the influence of external interference on the system. The second is the overall fuzzy adaptive sliding mode controller. Based on the function of the first controller, the adaptive fuzzy approximation of the fixed-wing UAV model is carried out. This controller can not only overcome the chattering problem but also eliminate the influence of external interference and internal uncertainty of the system.

The rest of this study is organized as follows: Section 2 describes the mathematical model of a fixed-wing UAV. Section 3 introduces fuzzy adaptive sliding mode controllers for attitude, airspeed, and altitude. Section 4 provides the simulation results and the related analysis of the above controllers using MATLAB. The conclusions are presented in the final section.

2. Mathematical Model

Before designing the controller, it is significant to establish proper mathematical models for the controlled object. This section describes the establishment of a kinematic and dynamic model for a fixed-wing UAV.

To maintain the generality of the kinematics and dynamics models of fixed-wing UAVs, the following assumptions need to be made before further analysis [24].

(i) Suppose the Earth has no rotation and revolution, and its curvature is zero.

(ii) The body of the fixed-wing UAV does not deform or vibrate when subjected to external forces, as it is rigid

(iii) The fuselage of the fixed-wing UAV is perfectly symmetrical about the central axis plane

The fixed-wing UAV has 12 degrees of freedom when operating; therefore, the mathematical model is complex. In order to obtain the complete mathematical model of a fixed-wing UAV, reference coordinates are necessary [24, 29]. These coordinate systems include the following:

(i) Ground inertial coordinate system ($O_G X_G Y_G Z_G$): the origin is the takeoff point of the UAV, X_G-axis points due north from the origin, and Y_G- axis points due east from the origin.

(ii) Body inertial coordinate system ($O_{Bi} X_{Bi} Y_{Bi} Z_{Bi}$): the origin is the center of mass of the UAV, and X_{Bi}-axis, Y_{Bi}-axis, and Z_{Bi}-axis are parallel to the ground inertial coordinate system.

(iii) Body coordinate system ($O_B X_B Y_B Z_B$): the origin is also the drone's center of mass, X_B- axis points to the nose from the origin, and Y_B-axis points from the origin towards the abdomen of the body.

(iv) Stable coordinate system ($O_S X_S Y_S Z_S$): the origin is still the drone's center of mass, X_S-axis points from the origin to the direction of the projection of the direction of the UAV motion in the longitudinal plane of symmetry, and Z_S-axis points to the right wing from the origin.

(v) Airflow coordinate system ($O_A X_A Y_A Z_A$): the origin is the center of gravity of the drone, X_A-axis points from the origin to the direction in which the drone is moving, and Z_A-axis points downward vertically with X_A-axis in the longitudinal symmetry plane of the UAV.

Above all, the following state quantities are defined in the ground coordinate system: P_x, P_y, P_z are the displacement states of the three axes. u, v, w represent the velocity of the displacement along the three axes. The Euler angles (Ψ, θ, Φ) are the angles at which the UAV body rotates on three axes, and their rate of change is denoted by (p, q, r).

$$\begin{pmatrix} \dot{P}_x \\ \dot{P}_y \\ \dot{P}_z \end{pmatrix} = \begin{pmatrix} \cos\Psi\cos\theta & \sin\Psi\cos\theta & -\sin\theta \\ -\cos\Phi\sin\Psi + \sin\Phi\sin\theta\cos\Psi & \cos\Phi\cos\Psi + \sin\Phi\sin\theta\sin\Psi & \cos\theta\sin\Phi \\ \sin\Phi\sin\Psi + \cos\Phi\sin\theta\cos\Psi & -\sin\theta\cos\Psi + \cos\Phi\sin\theta\cos\Psi & \cos\theta\cos\Phi \end{pmatrix}^T \begin{pmatrix} u \\ v \\ w \end{pmatrix},$$
$$\begin{pmatrix} \dot{\Psi} \\ \dot{\theta} \\ \dot{\Phi} \end{pmatrix} = \begin{pmatrix} 1 & \sin\Phi\tan\theta & \cos\Phi\tan\theta \\ 0 & \cos\Phi & -\sin\Phi \\ 0 & \sin\Phi\sec\theta & \cos\Phi\sec\theta \end{pmatrix} \begin{pmatrix} p \\ q \\ r \end{pmatrix}. \tag{1}$$

This chapter establishes a mathematical model of a fixed-wing UAV based on the body coordinate system. The position and attitude kinematics models of the fixed-wing UAV can be obtained through the transformation relationship between different coordinate systems [30, 31] as follows: Ψ is the yaw angle, θ is the pitch angle, and Φ is the roll angle.

Then, the initial force analysis of the fixed-wing UAV is carried out.

Using Newton's second law as the basis for force analysis,

$$F = \frac{\mathrm{d}}{\mathrm{d}t}mV, \qquad M = \frac{\mathrm{d}}{\mathrm{d}t}H, \tag{2}$$

where F is the accumulation of external forces, m is the mass of the UAV, M is the accumulation of torques, and H is the angular momentum.

Expand these two formulas according to the force conditions to obtain the dynamic model related to the displacement acceleration and angular acceleration of the fixed-wing UAV [31]:

$$\begin{pmatrix} \dot{u} \\ \dot{v} \\ \dot{w} \end{pmatrix} = \begin{pmatrix} -qw + rv \\ -ru + pw \\ -pv + qu \end{pmatrix} + \frac{1}{m}\begin{pmatrix} f_x \\ f_y \\ f_z \end{pmatrix},$$
$$\begin{pmatrix} \dot{p} \\ \dot{q} \\ \dot{r} \end{pmatrix} = \begin{pmatrix} T_1pq - T_2qr + T_3t_1 + T_4t_3 \\ T_5pr - T_6\left(p^2 - r^2\right) + \frac{1}{j_y}t_2 \\ T_7pq - T_1qr + T_4t_1 + T_8t_3 \end{pmatrix}, \tag{3}$$

where $j_x = \int (z^2 + y^2)\mathrm{d}m$, $j_y = \int (z^2 + y^2)\mathrm{d}m$, $j_z = \int (y^2 + x^2)\mathrm{d}m$, $j_{xy} = \int xy\mathrm{d}m$, $j_{xz} = \int xz\mathrm{d}m$, $j_{yz} = \int yz\mathrm{d}m$, $T = j_xj_y - j_{xz}^2$, $T_1 = j_{xz}(j_x - j_y + j_z)/T$, $T_2 = j_z(j_z - j_y) + j_{xz}^2/T$, $T_3 = 1j_z/T$, $T_4 = j_{xz}/T$, $T_5 = j_z - j_x/j_z$, $T_6 = j_{xz}/j_y$, $T_7 = j_x(j_x - j_y) + j_{xz}^2/T$, and $T_8 = j_x/T$. t_1, t_2, t_3 are the projections of the torque on the three axes of the body coordinate system.

Preliminary force analysis was completed. Before designing the controller, the forces in the above model must be related to the output of the motor of the fixed-wing UAV; therefore, it is necessary to conduct further analysis to obtain the relevant aerodynamic and thrust models.

First, the force of the fixed-wing UAV was analyzed longitudinally. In the longitudinal plane, the state quantities leading the UAV movement are mainly the lift force (f_{up}), drag force (f_r), and moment of inertia of rotation around the vector pointing to the wing (t_1). These can be represented by the following formulas:

$$f_{\mathrm{up}} = \frac{1}{2}\rho V_a^2 \mathrm{S}C_L(\alpha, q, U_1),$$
$$f_r = \frac{1}{2}\rho V_a^2 \mathrm{S}C_D(\alpha, q, U_1), \tag{4}$$
$$t_2 = \frac{1}{2}\rho V_a^2 ScC_m(\alpha, q, U_1),$$

where c is the average aerodynamic chord length, ρ is the air density, S is the UAV wing area, C_L is the lift coefficient, C_D is the drag coefficient, C_D is the moment coefficient, U_1 is the elevator command signal, α is the attack angle, and β is the sideslip angle.

When the attack angle is small, the aerodynamic parameters above can be linearized using the first-order Taylor formula. The following results were obtained:

$$f_{\mathrm{up}} = \frac{1}{2}\rho V_a^2 S\left(C_L(\alpha) + C_{Lq}\frac{c}{2V_a}q + C_{\mathrm{LU}_1}U_1\right),$$
$$f_r = \frac{1}{2}\rho V_a^2 S\left(C_D(\alpha) + C_{Dq}\frac{c}{2V_a}q + C_{\mathrm{DU}_1}U_1\right), \tag{5}$$
$$t_2 = \frac{1}{2}\rho V_a^2 Sc\left(C_{t_2}(\alpha) + C_{t_2q}\frac{c}{2V_a}q + C_{t_2U_1}U_1\right),$$

where $C_L(\alpha)$, $C_D(\alpha)$, and $C_{t_2}(\alpha)$ are the nonlinear equations related to α with different coefficients, $C_{Lq} \triangleq \partial C_L/\partial q$, $C_{\mathrm{LU}_1} \triangleq \partial C_L/\partial U_1$, $C_{Dq} \triangleq \partial C_D/\partial q$, $C_{\mathrm{LU}_1} \triangleq \partial C_D/\partial U_1$, $C_{t_2q} \triangleq \partial C_{t_2}/\partial q$, and $C_{t_2U_1} \triangleq \partial C_{t_2}/\partial U_1$.

Because the type of f_{up} and f_r is defined in the stability of the system, they need to be transformed into ontological coordinates.

$$\begin{pmatrix} f_x \\ f_z \end{pmatrix} = \begin{pmatrix} \cos\alpha & -\sin\alpha \\ \sin\alpha & \cos\alpha \end{pmatrix} \begin{pmatrix} -f_{\text{up}} \\ -f_r \end{pmatrix}$$
$$= \frac{1}{2}\rho V_a^2 S \begin{pmatrix} [C_L(\alpha)\sin\alpha - C_D(\alpha)\cos\alpha] + \left[C_{Lq}\sin\alpha - C_{Dq}\cos\alpha\right]\dfrac{c}{2V_a}q + \left[C_{\text{LU}_1}\sin\alpha - C_{\text{DU}_1}\cos\alpha\right] \\ [-C_L(\alpha)\cos\alpha - C_D(\alpha)\sin\alpha] + \left[-C_{Dq}\sin\alpha - C_{Lq}\cos\alpha\right]\dfrac{c}{2V_a}q + \left[-C_{\text{LU}_1}\cos\alpha - C_{\text{DU}_1}\sin\alpha\right] \end{pmatrix}. \tag{6}$$

In the transverse plane, the state quantities that dominate the UAV motion are the rudder (U_2), aileron steering gear (U_3), yaw angular velocity (p), roll angular velocity (r), and sideslip angle (β). Their relationships are as follows:

$$\begin{aligned} f_y &= \frac{1}{2}\rho V_a^2 \text{SC}_Y(\beta, p, r, U_2, U_3), \\ t_1 &= \frac{1}{2}\rho V_a^2 SbC_{t_1}(\beta, p, r, U_2, U_3), \\ t_3 &= \frac{1}{2}\rho V_a^2 SbC_{t_3}(\beta, p, r, U_2, U_3), \end{aligned} \tag{7}$$

where C_Y is the dimensionless lateral force coefficient, C_{t_1} is the dimensionless rolling moment coefficient, and C_{t_3} is the dimensionless yaw moment coefficient.

They are also linearized by the first-order Taylor formula to get

$$\begin{aligned} f_y &= \frac{1}{2}\rho V_a^2 S\left(C_{Y_0} + C_{Y_\beta}\beta + C_{Y_p}\frac{b}{2V_a}p + C_{Y_r}\frac{b}{2V_a}r + C_{\text{YU}_2}U_2 + C_{\text{YU}_3}U_3\right), \\ t_1 &= \frac{1}{2}\rho V_a^2 Sb\left(C_{t_{10}} + C_{t_{1\beta}}\beta + C_{t_{1p}}\frac{b}{2V_a}p + C_{t_{1r}}\frac{b}{2V_a}r + C_{t_1U_2}U_2 + C_{t_1U_3}U_3\right), \\ t_3 &= \frac{1}{2}\rho V_a^2 Sb\left(C_{t_{30}} + C_{t_{3\beta}}\beta + C_{t_{3p}}\frac{b}{2V_a}p + C_{t_{3r}}\frac{b}{2V_a}r + C_{t_3U_2}U_2 + C_{t_3U_3}U_3\right). \end{aligned} \tag{8}$$

The core propulsion force of the fixed-wing UAV can be expressed as

$$F = \frac{1}{2}\rho S_p C_p\left[(k_m U_4)^2 - V_a^2\right], \tag{9}$$

where S_p is the area swept by the propeller, C_p is the thrust-related parameter, k_m is the propeller engine parameter, and U_4 is the propeller engine acceleration.

By integrating all the mathematical models above, a complete mathematical model of a fixed-wing UAV can be obtained as follows:

$$\begin{aligned} \dot{P}_x &= \cos\Psi\cos\theta u + (-\cos\Phi\sin\Psi + \sin\Phi\sin\theta\cos\Psi)v + (\sin\Phi\sin\Psi + \cos\Phi\sin\theta\cos\Psi)w, \\ \dot{P}_y &= \sin\Psi\cos\theta u + (\cos\Phi\cos\Psi + \sin\Phi\sin\theta\sin\Psi)v + (-\sin\theta\cos\Psi + \cos\Phi\sin\theta\cos\Psi)w, \\ \dot{P}_z &= \sin\theta u - \cos\theta\sin\Phi v - \cos\theta\cos\Phi w, \\ \dot{\Psi} &= \sin\Phi\sec\theta q + \cos\Phi\sec\theta r, \\ \dot{\theta} &= \cos\Phi q - \sin\Phi r, \\ \dot{\Phi} &= p + \sin\Phi\tan\theta q + \cos\Phi\tan\theta r, \end{aligned}$$

$$
\begin{aligned}
\dot{u} &= rv - qw - g\sin\theta + \frac{1}{2m}\rho V_a^2 S\left[C_1(\alpha) + C_2(\alpha)\frac{cq}{2V_a} + C_3(\alpha)U_1\right] + \frac{1}{2m}\rho S_p C_p\left[(k_m U_4)^2 - V_a^2\right],\\
\dot{v} &= -ru + pw + g\cos\theta\sin\Phi + \frac{1}{2m}\rho V_a^2 S\left[C_{Y_0} + C_{Y_\beta}\beta + C_{Y_p}\frac{bp}{2V_a} + C_{Y_r}\frac{br}{2V_a} + C_{YU_2}U_2 + C_{YU_3}U_3\right],\\
\dot{w} &= -pv + qu + g\cos\theta\sin\Phi + \frac{1}{2m}\rho V_a^2 S\left[C_4(\alpha) + C_5(\alpha)\frac{cq}{2V_a} + C_6(\alpha)U_1\right],\\
\dot{p} &= T_1 pq - T_2 qr + \frac{1}{2}\rho V_a^2 Sb\left(C_7 + C_8\beta + C_9\frac{b}{2V_a}p + C_{10}\frac{b}{2V_a}r + C_{11}U_2 + C_{12}U_3\right),\\
\dot{q} &= T_5 pr - T_6\left(p^2 - r^2\right) + \frac{1}{2j_y}\rho V_a^2 Sc\left(C_{t_2}(\alpha) + C_{t_2 q}\frac{c}{2V_a}q + C_{t_2U_1}U_1\right),\\
\dot{r} &= T_7 pq - T_1 qr + \frac{1}{2}\rho V_a^2 Sb\left(C_{13} + C_{14}\beta + C_{15}\frac{b}{2V_a}p + C_{16}\frac{b}{2V_a}r + C_{17}U_2 + C_{18}U_3\right),
\end{aligned}
\tag{10}
$$

where $C_1(\alpha) \triangleq C_L(\alpha)\sin\alpha - C_D(\alpha)\cos\alpha$, $C_2(\alpha) \triangleq C_{Lq}\sin\alpha - C_{Dq}\cos\alpha$, $C_3(\alpha) \triangleq C_{\mathrm{LU}_1}\sin\alpha - C_{\mathrm{DU}_1}\cos\alpha$, $C_4(\alpha) \triangleq -C_L(\alpha)\cos\alpha - C_D(\alpha)\sin\alpha$, $C_5(\alpha) \triangleq -C_{Dq}\sin\alpha - C_{Lq}\cos\alpha$, $C_6(\alpha) \triangleq -C_{\mathrm{LU}_1}\cos\alpha - C_{\mathrm{DU}_1}\sin\alpha$, $C_7 = T_3 C_{t_{10}} + T_4 C_{t_{30}}$, $C_8 = T_3 C_{t_{1\beta}} + T_4 C_{t_{3\beta}}$, $C_9 = T_3 C_{t_{1p}} + T_4 C_{t_{3p}}$, $C_{10} = T_3 C_{t_{1r}} + T_4 C_{t_{3r}}$, $C_{11} = T_3 C_{t_1 U_1} + T_4 C_{t_3 U_1}$, $C_{12} = T_3 C_{t_1 U_2} + T_4 C_{t_3 U_2}$, $C_{13} = T_4 C_{t_{10}} + T_8 C_{t_{30}}$, $C_{14} = T_4 C_{t_{1\beta}} + T_8 C_{t_{3\beta}}$, $C_{15} = T_4 C_{t_{1p}} + T_8 C_{t_{3p}}$, $C_{16} = T_4 C_{t_{1r}} + T_8 C_{t_{3r}}$, $C_{17} = T_4 C_{t_1 U_1} + T_8 C_{t_3 U_1}$, and $C_{18} = T_4 C_{t_1 U_2} + T_8 C_{t_3 U_2}$.

Precise modeling of the fixed-wing UAV has been completed. However, it is not necessary for one of two controllers designed as follows. The fuzzy adaptive sliding mode controller for switching term only needs accurate modeling information, while the comprehensive fuzzy adaptive sliding mode controller does not need an accurate mathematical model in the process of controller design due to its ability to perform fuzzy approximation to the model of the controlled object.

3. Controller Design

This chapter describes the controller design process of a fixed-wing UAV based on the above mathematical models. The fixed-wing UAV model is a typical nonlinear system that is characterized by multiple inputs, multiple outputs, strong coupling, and under actuation. Therefore, this study introduces a new coupling control method that focuses on the fixed-wing UAV control problem. This method is based on sliding mode control and combines fuzzy control and adaptive control methods. The sliding mode control part is mainly used to deal with the control difficulties caused by complex nonlinear models, and the adaptive law is introduced to solve the multiple uncertainties of fixed-wing UAVs in operation. In addition, the chattering caused by the sliding mode control was eliminated through the fuzzy control method.

Before designing the specific controller, we first need to design the control flow. A typical fixed-wing UAV has 12 degrees of freedom, and it is very complicated to control and track all degrees of freedom simultaneously. Because the fixed-wing UAV is in a state of high-speed movement when working, the precise control of a part of the degrees of freedom is meaningless. In this study, five degrees of freedom were selected for tracking and control to meet the requirements of daily tasks. These five state variables include three attitude angles, airspeed, and flight altitude. According to this control idea, a control system with attitude control and airspeed control as two inner loops and flight altitude control as an outer loop is designed as shown in Figure 1.

The control command signal source provides instructions for seven state variables, including three attitude angles transmitted to the attitude fuzzier, three speed states transmitted to the velocity fuzzier along three axes in the body coordinate system, and one flight altitude transmitted to the altitude solver. The inner loop control system includes attitude control and airspeed control. The attitude blurrier and speed blurrier calculate the target errors by processing the command signal, and the corresponding controller realizes the control process of the respective state quantity after receiving the error signals. The control inputs of the attitude angles are U_1, U_2, and U_3, whereas the airspeed control process mainly depends on U_4. The height control system is the outer loop control system, which is combined with an inner control loop to realize the height control process. The main control idea of the outer control loop is to select the control mode and determine the required secondary control signals after receiving instruction of h_d. This is explained in detail in Section 3.3.

3.1. Attitude Controller Design. In the second chapter, all kinematic and dynamic models of the attitude angles are obtained. It is clear that these mathematical models are still very complex. To simplify the control process, it is necessary to decouple the mathematical models before designing the attitude controllers.

Decoupling processing is mainly to extract the dominant state quantity in the control process and treat the remaining control quantity as uncertainty [32]. Based on this, related mathematical models can be conducted as follows:

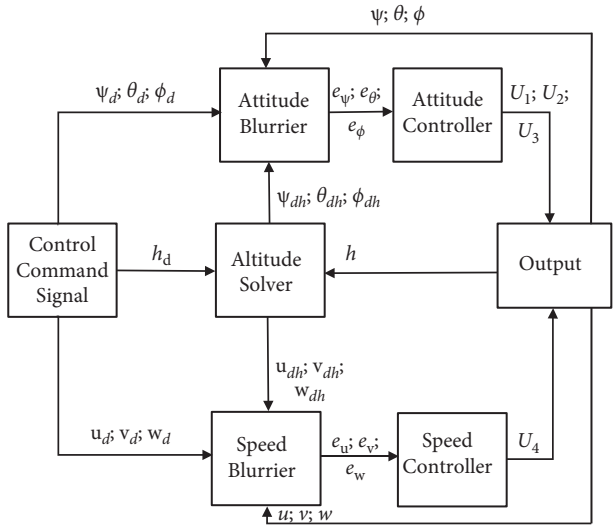

Figure 1: Control inner loop and outer loop.

$$
\begin{aligned}
\ddot{\Psi} &= T_7 pq - T_1 qr + \frac{1}{2}\rho V_a^2 Sb\left(C_{13} + C_{14}\beta + C_{15}\frac{b}{2V_a}p + C_{16}\frac{b}{2V_a}r + C_{17}U_2 + C_{18}U_3\right) + \dot{d}_{\Psi 1} \\
&= T_7 pq - T_1 qr + \frac{1}{2}\rho V_a^2 Sb\left(C_{13} + C_{14}\beta + C_{15}\frac{b}{2V_a}p + C_{16}\frac{b}{2V_a}\left(\dot{\Psi} - d_{\Psi 1}\right) + C_{17}U_2 + C_{18}U_3\right) + \dot{d}_{\Psi 1} \\
&= a_{\Psi 1}\dot{\Psi} + a_{\Psi 2}U_2 + d_{\Psi}, \\
\ddot{\theta} &= T_5 pr - T_6\left(p^2 - r^2\right) + \frac{1}{2j_y}\rho V_a^2 Sc\left\{C_{t_{20}} + C_{t_{21}}(\theta - \varepsilon) + C_{t_2 q}\frac{c}{2V_a}q + C_{t_{2U_1}}U_1\right\} + \dot{d}_{\theta 1} \\
&= a_{\theta 1}\dot{\theta} + a_{\theta 2}\theta + a_{\theta 3}U_1 + d_{\theta}, \\
\ddot{\Phi} &= T_1 pq - T_2 qr + \frac{1}{2}\rho V_a^2 Sb\left(C_7 + C_8\beta + C_9\frac{b}{2V_a}p + C_{10}\frac{b}{2V_a}r + C_{11}U_2 + C_{12}U_3\right) + \dot{d}_{\Phi 1} \\
&= a_{\Phi 1}\dot{\Phi} + a_{\Phi 2}U_3 + d_{\Phi},
\end{aligned}
\tag{11}
$$

where $a_{\Psi 1} = (1/2)\rho V_a^2 SbC_{16}(b/2V_a)$, $a_{\Psi 2} = (1/2)\rho V_a^2 SbC_{17}$, $a_{\theta 1} = (1/2j_y)\rho V_a^2 SC_{t_2 q}(C^2/2V_a)$, $a_{\theta 2} = (1/2j_y)\rho V_a^2 ScC_{t_{21}}$, $a_{\theta 3} = (1/2j_y)\rho V_a^2 ScC_{t_{2U_1}}$, $a_{\Phi 1} = (1/2)\rho V_a^2 SbC_9(b/2V_a)$, $a_{\Phi 2} = (1/2)\rho V_a^2 SbC_{12}$, and d_{Ψ}, d_{θ}, and d_{Φ} are defined as the total uncertainties: $d_{\Psi} = T_7 pq - T_1 qr + (1/2)\rho V_a^2 Sb(C_{13} + C_{14}\beta + C_{15}b/2V_a p - C_{16}2V_a/bd_{\Psi 1} + C_{18}U_3) + \dot{d}_{\Psi 1}$, $d_{\theta} = T_5 pr - T_6(p^2 - r^2) + (1/2j_y)\rho V_a^2 Sc(C_{t_{20}} - C_{t_{21}}\varepsilon - C_{t_2 q}c/2V_a d_{\theta 1}) + \dot{d}_{\theta 1}$, and $d_{\Phi} = T_1 pq - T_2 qr + (1/2)\rho V_a^2 Sb(C_7 + C_8\beta - C_9 b/2V_a d_{\theta 1} + C_{10}b/2V_a + C_{11}U_2) + \dot{d}_{\Phi 1}$.

After sorting, we can get

$$
\begin{cases}
\dot{X} = A(X) + B(X)U = \begin{cases} x_2, \\ a_{\Psi 1}x_2 + a_{\Psi 2}U_2 + d_{\Psi}, \\ x_4, \\ a_{\theta 1}x_4 + a_{\theta 2}x_3 + a_{\theta 3}U_1 + d_{\theta}, \\ x_6, \\ a_{\Phi 1}x_6 + a_{\Phi 2}U_3 + d_{\Phi}, \end{cases} \\
Y = C(X).
\end{cases}
\tag{12}
$$

Take the yaw angle control system as an example.

Rewrite the equation of state in the following form:

$$\begin{aligned}\dot{x}_1 &= x_2,\\ \dot{x}_2 &= f_\Psi(x_1,t) + g_\Psi(x_1,t)U_2 + d_\Psi,\\ y &= x_1.\end{aligned} \tag{13}$$

First, a simple switching fuzzification adaptive sliding mode control is designed (only the switching item is blurred).

Let us treat $f_\Psi(x_1,t)$ and $g_\Psi(x_1,t)$ as the known nonlinear functions, $x_1 \in R^n$, $x_2 \in R$, $U_2 \in R$, and d_Ψ is the unknown interference, $|d_\Psi| \le D_\Psi$, $g(x_1,t) > 0$.

Define $z_{\Psi 1} = x_1 - x_{1\,d}$ as the systematic error:

$$z_{\Psi 2} = \dot{z}_{\Psi 1} = \dot{x}_1 - \dot{x}_{1\,d}. \tag{14}$$

The sliding surface is defined as follows.

$$\tau_\Psi = k_{\Psi 1} z_{\Psi 1} + z_{\Psi 2}, \tag{15}$$

where $k_{\Psi 1} > 0$.

Substituting equation (14) into (15), we can get

$$\begin{aligned}\tau_\Psi &= k_{\Psi 1} z_{\Psi 1} + z_{\Psi 2}\\ &= k_{\Psi 1} z_{\Psi 1} + \dot{x}_1 - \dot{x}_{1\,d}.\end{aligned} \tag{16}$$

Design sliding mode control law:

$$\begin{aligned}U_2 &= \frac{1}{g_\Psi(x_1,t)}\left[-f_\Psi(x_1,t) - k_{\Psi 1} z_{\Psi 2} + \ddot{x}_{1\,d} - U_{\Psi sw}\right]\\ &= \frac{1}{a_{\Psi 2}}\left[-a_{\Psi 1}x_2 - k_{\Psi 1} z_{\Psi 2} + \ddot{x}_{1\,d} - U_{\Psi sw}\right],\end{aligned} \tag{17}$$

where $U_{\Psi sw} = \eta_\Psi \mathrm{sgn}(\tau_\Psi)$, $\eta_\Psi > 0$.

Taking the derivative of equation (16),

$$\begin{aligned}\dot{\tau}_\Psi &= k_{\Psi 1}\dot{z}_{\Psi 1} + \ddot{x}_1 - \ddot{x}_{1\,d}\\ &= k_{\Psi 1}\dot{z}_{\Psi 1} + \dot{x}_2 - \ddot{x}_{1\,d}\\ &= k_{\Psi 1}\dot{z}_{\Psi 1} + a_{\Psi 1}x_2 + a_{\Psi 2}U_2 + d_\Psi - x_d.\end{aligned} \tag{18}$$

Substitute equation (17) into (18) to obtain

$$\begin{aligned}\dot{\tau}_\Psi &= k_{\Psi 1}\dot{z}_{\Psi 1} + a_{\Psi 1}x_2 + a_{\Psi 2}\left\{\frac{1}{a_{\Psi 2}}\left[-a_{\Psi 1}x_2 - k_{\Psi 1}z_{\Psi 2} + \ddot{x}_d - U_{\Psi sw}\right]\right\} + d_\Psi - \ddot{x}_d\\ &= d_\Psi - U_{\Psi sw},\\ \tau_\Psi\dot{\tau}_\Psi &= \tau_\Psi d_\Psi - \tau_\Psi U_{\Psi sw}\\ &= \tau_\Psi d_\Psi - \tau_\Psi\eta_\Psi\mathrm{sgn}(\tau_\Psi)\\ &= \tau_\Psi d_\Psi - \eta_\Psi|\tau_\Psi|.\end{aligned} \tag{19}$$

To satisfy the condition of stability ($\tau_\Psi d_\Psi - \eta_\Psi|\tau_\Psi| \le 0$), when the interference item d_Ψ is a larger value, the switch gain η in the controller should be larger, which is the main reason for shaking. To reduce chattering, the fuzzy system $\hat{\eta}_\Psi$ is designed to approximate $\eta_\Psi\mathrm{sgn}(\tau_\Psi)$.

The fuzzy system is designed using a product inference machine, a single-valued fuzzier, and a central average fuzzier [33]. The output of the fuzzy system is $\hat{\eta}_\Psi$. Then, the control law can be rewritten as follows:

$$\begin{aligned}U_2 &= \frac{1}{a_{\Psi 2}}\left[-a_{\Psi 1}x_2 - k_{\Psi 1}z_{\Psi 2} + \ddot{x}_{1\,d} - \hat{\eta}_\Psi(\tau_\Psi)\right],\\ \hat{\boldsymbol{\eta}}_\Psi\left(\tau_\Psi|\hat{\boldsymbol{\zeta}}_{\eta_\Psi}\right) &= \hat{\boldsymbol{\zeta}}_{\eta_\Psi}^{T}\varrho(\tau_\Psi),\end{aligned} \tag{20}$$

where $\hat{\eta}_\Psi(\tau_\Psi|\hat{\zeta}_\eta)$ is the output of the fuzzy system, $\boldsymbol{\varrho}(\tau_\Psi)$ is a fuzzy vector, and vector $\hat{\zeta}_\eta^{T}$ varies according to the adaptive law.

The ideal $\hat{\eta}_\Psi(\tau_\Psi|\zeta_\eta)$ is

$$\hat{\boldsymbol{\eta}}_\Psi\left(\tau_\Psi|\zeta_\eta^*\right) = \eta_\Psi\mathrm{sgn}(\tau_\Psi), \tag{21}$$

where ζ_η^* is the optimal parameter, $\eta_\Psi > D_\Psi$.

The adaptive law can be designed as

$$\dot{\hat{\zeta}}_{\eta_\Psi} = \gamma_\Psi\tau_\Psi\varrho(\tau_\Psi), \tag{22}$$

where $\gamma_\Psi > 0$.

It is worth noting that in traditional sliding mode control, the convergence rate of the controlled system is mainly determined by the switching term. In the above design, the switching term is replaced by a fuzzy adaptive step. Therefore, under the action of the controller, the convergence speed of the system depends on the size of membership function and adaptive parameters in the fuzzy adaptive part.

Similarly, for other attitude angles θ and Φ, the following control laws and adaptive laws can be designed, as given in Table 1.

In practice, f and g are often unable to be determined owing to multiple disturbances. Based on the above, adaptive fuzzy laws are designed to approximate f and g.

The attitude angle Ψ control system was also taken as an example for the analysis. If $f_\Psi(x_1,t)$ and $g_\Psi(x_1,t)$ are unknown, it is necessary to add the design fuzzy system $\hat{f}_\Psi$ and $\hat{g}_\Psi$ to approximate f_Ψ and g_Ψ.

Table 1: The simple control laws and adaptive laws of θ and Φ.

Items	θ	Φ
Systematic error	$z_{\theta 1} = x_3 - x_{3\,d}$	$z_{\Phi 1} = x_5 - x_{5\,d}$
Control input	$U_1 = 1/a_{\theta 3}[-(a_{\theta 1}x_4 + a_{\theta 2}x_3) - k_{\theta 1}z_{\theta 2} + \ddot{x}_{3\,d} - \hat{\eta}_\theta(\tau_\theta)]$	$U_3 = 1/a_{\Phi 2}[-a_{\Phi 1}x_6 - k_{\Phi 1}z_{\Phi 2} + \ddot{x}_{5\,d} - \hat{\eta}_\Phi(\tau_\Phi)]$
Sliding surface	$\tau_\theta = k_{\theta 1}z_{\theta 1} + z_{\theta 2}$	$\tau_\Phi = k_{\Phi 1}z_{\Phi 1} + z_{\Phi 2}$
Fuzzy system output	$\hat{\eta}_\theta(\tau_\theta \mid \hat{\zeta}_{\eta\theta}) = \hat{\zeta}_{\eta\theta}^T \varrho(\tau_\theta)$	$\hat{\eta}_\Phi(\tau_\Phi \mid \hat{\zeta}_{\eta\Phi}) = \hat{\zeta}_{\eta\Phi}^T \boldsymbol{\varrho}(\tau_\Phi)$
Adaptive law	$\dot{\hat{\zeta}}_{\eta\theta} = \gamma_\theta \tau_\theta \varrho(\tau_\theta)$	$\dot{\hat{\zeta}}_{\eta\Phi} = \gamma_\Phi \tau_\Phi \varrho(\tau_\Phi)$

The product inference machine, single-valued fuzzier, and central average fuzzy solution were used to design the fuzzy system. The outputs of the fuzzy system are, respectively, $\hat{f}_\Psi$, $\hat{g}_\Psi$, and $\hat{\eta}_\Psi$. The control law can then be rewritten as follows:

$$U_2 = \frac{1}{\hat{g}_\Psi(x_1, t)}\left[-\hat{f}_\Psi(x_1, t) - k_{\Psi 1}z_{\Psi 2} + \ddot{x}_{1\,d} - \hat{\eta}_\Psi(\tau_\Psi)\right], \tag{23}$$

$$\begin{aligned}
\hat{f}_\Psi\left(x_1 \mid \boldsymbol{\zeta}_{f_\Psi}\right) &= \hat{\boldsymbol{\zeta}}_{f_\Psi}^T \boldsymbol{\xi}(\tau_\Psi),\\
\hat{g}_\Psi\left(x_1 \mid \boldsymbol{\zeta}_{g_\Psi}\right) &= \hat{\boldsymbol{\zeta}}_{g_\Psi}^T \boldsymbol{\xi}(\tau_\Psi),\\
\hat{\eta}_\Psi\left(\tau_\Psi \mid \boldsymbol{\zeta}_{\eta_\Psi}\right) &= \hat{\boldsymbol{\zeta}}_{\eta_\Psi}^T \boldsymbol{\varrho}(\tau_\Psi),
\end{aligned} \tag{24}$$

where $\hat{f}_\Psi(x_1 \mid \hat{\zeta}_f)$, $\hat{g}_\Psi(x_1)$, and $\hat{\eta}_\Psi(\tau_\Psi \mid \hat{\zeta}_{\eta_\Psi})$ are the outputs of the fuzzy system, $\xi(\tau_\Psi)$ and $\boldsymbol{\varrho}(\tau_\Psi)$ are the fuzzy vectors, and vectors $\zeta_{\mathbf{f}}^{\mathbf{T}}$, $\zeta_{\mathbf{g}}^{\mathbf{T}}$, and $\zeta_\eta^{\mathbf{T}}$ vary according to the adaptive law.

$$\begin{aligned}
\hat{\eta}_\Psi\left(\tau_\Psi \mid \hat{\boldsymbol{\zeta}}_{\eta_\Psi}\right) &= \eta_{\Delta\Psi}\mathrm{sgn}(\tau_\Psi),\\
\eta_{\Delta\Psi} &= D_\Psi + \eta_\Psi,\ \eta_\Psi > 0.
\end{aligned} \tag{25}$$

The adaptive law for f and g can be designed as

$$\begin{aligned}
\dot{\hat{\zeta}}_{f_\Psi} &= \gamma_{1\Psi}\tau_\Psi \xi(x_1),\\
\dot{\hat{\zeta}}_{g_\Psi} &= \gamma_{2\Psi}\tau_\Psi \xi(x_1)U_2.
\end{aligned} \tag{26}$$

The adaptive law for switch item is still

$$\dot{\hat{\zeta}}_{\eta_\Psi} = \gamma_\Psi \tau_\Psi \varrho(\tau_\Psi). \tag{27}$$

It can be seen that a high precision mathematical model is not necessary in the design process of this controller because its adaptive fuzzy part can approximate the controlled object model. Rough mathematical models are sufficient to select membership functions required by the T-S fuzzy method.

Similarly, for attitude angles θ and Φ, the following control laws and adaptive laws can be designed as given in Table 2.

3.2. Airspeed. The airspeed of the fixed-wing UAV, which is the sum of the velocity vectors in the three-axis directions in the body coordinate system, can be expressed as

$$V_a = \sqrt{u^2 + v^2 + w^2}. \tag{28}$$

When the airspeed controller is operating, velocities in directions other than the X_G-axis can be treated as disturbances. Therefore, the expression of air speed can be transformed into the following form:

$$V_a = u + d_{V_a 1}, \tag{29}$$

where $d_{V_a 1}$ is the perturbation of the Y-axis and Z-axis velocities in the body coordinate system.

By decoupling the above equation according to the relevant mathematical model, the following can be obtained:

$$\begin{aligned}
\ddot{V}_a &= \frac{1}{m}\rho S C_1(\alpha)V_a + \frac{1}{4m}\rho S C_2(\alpha)cq\dot{V}_a + \frac{1}{m}\rho S C_3(\alpha)U_1 V_a + \frac{1}{m}\rho S_p C_p k_m^2 U_4 - \frac{1}{m}\rho S_p C_p V_a + \dot{d}_{V_a 2}\\
&= a_{V_a 1}V_a + a_{V_a 2}\dot{V}_a + a_{V_a 3}U_4 + \dot{d}_{V_a 2},
\end{aligned} \tag{30}$$

where $a_{V_a 1} = (1/m)\rho S C_1(\alpha) + (1/m)\rho S C_3(\alpha)U_1 - (1/m)\rho S_p C_p$, $a_{V_a 2} = (1/4m)\rho S C_2(\alpha)cq$; $a_{V_a 3} = (1/m)\rho S_p C_p k_m^2$, and $d_{V_a 2} = rv - qw - g\sin\theta + \dot{d}_{V_a 1}$.

Define $x_7 = V_a$, $x_8 = \dot{V}_a$, and the state space function is

$$\begin{cases}
\dot{x}_7 = x_8,\\
\dot{x}_8 = a_{V_a 1}x_7 + a_{V_a 2}x_8 + a_{V_a 3}U_4 + D_{V_a},\\
y_7 = x_7,
\end{cases} \tag{31}$$

where $D_{V_a} = \Delta a_{V_a 1}x_7 + \Delta a_{V_a 2}x_8 + \Delta a_{V_a 3}U_4 + \dot{d}_{V_a 2}$ is the total uncertainty.

Similar to the attitude controller design, the control law and adaptive law of airspeed can be obtained as follows:

(i) When f and g are acknowledged nonlinear functions, the control law, sliding surface, fuzzy system output, and adaptive law can be designed as

Table 2: The complex control laws and adaptive laws of θ and Φ.

Items	θ	Φ
Systematic error	$z_{\theta 1} = x_3 - x_{3\,d}$	$z_{\Phi 1} = x_5 - x_{5\,d}$
Control input	$U_1 = 1/\hat{g}_\theta(x_3,t)[-\hat{f}_\theta(x_3,t) - k_{\theta 1}z_{\theta 2} + \ddot{x}_{3\,d} - \hat{\eta}_\theta(\tau_\theta)]$	$U_3 = 1/\hat{g}_\Phi(x_5,t)[-\hat{f}_\Phi(x_5,t) - k_{\Phi 1}z_{\Phi 2} + \ddot{x}_{5\,d} - \hat{\eta}_\Phi(\tau_\Phi)]$
Sliding surface	$\tau_\theta = k_{\theta 1}z_{\theta 1} + z_{\theta 2}$	$\tau_\Phi = k_{\Phi 1}z_{\Phi 1} + z_{\Phi 2}$
Fuzzy system output	$\hat{f}_\theta(x_3 \mid \zeta_{f_\theta}) = \hat{\zeta}_{f_\theta}^T \xi(\tau_\theta)$ $\hat{g}_\theta(x_3 \mid \zeta_{g_\theta}) = \hat{\zeta}_{g_\theta}^T \xi(\tau_\theta)$ $\hat{\eta}_\theta(\tau_\theta \mid \hat{\zeta}_{\eta\theta}) = \hat{\zeta}_{\eta\theta}^T \varrho(\tau_\theta)$	$\hat{f}_\Phi(x_5 \mid \zeta_{f_\Phi}) = \hat{\zeta}_{f_\Phi}^T \xi(\tau_\Phi)1$ $\hat{g}_\Phi(x_5 \mid \zeta_{g_\Phi}) = \hat{\zeta}_{g_\Phi}^T \xi(\tau_\Phi)$ $\hat{\eta}_\Phi(\tau_\Phi \mid \hat{\zeta}_{\eta\Phi}) = \hat{\zeta}_{\eta\Phi}^T \varrho(\tau_\Phi)$
Adaptive law	$\dot{\hat{\zeta}}_{f_\theta} = \gamma_{1\theta}\tau_\theta \xi(x_3)$ $\dot{\hat{\zeta}}_{g_\theta} = \gamma_{2\theta}\tau_\theta \xi(x_3)U_1$ $\dot{\hat{\zeta}}_{\eta\theta} = \gamma_\theta \tau_\theta \varrho(\tau_\theta)$	$\dot{\hat{\zeta}}_{f_\Phi} = \gamma_{1\Phi}\tau_\Phi \xi(x_5)$ $\dot{\hat{\zeta}}_{g_\Phi} = \gamma_{2\Phi}\tau_\Phi \xi(x_5)U_3$ $\dot{\hat{\zeta}}_{\eta\Phi} = \gamma_\Phi \tau_\Phi \varrho(\tau_\Phi)$

$$
\begin{aligned}
U_4 &= \frac{1}{a_{V_a 3}}\left[-\left(a_{V_a 1}x_7 + a_{V_a 2}x_8\right) - k_{V_a 1}z_{V_a 2}\right.\\
&\quad \left. + \ddot{x}_{7\,d} - \hat{\eta}_{V_a}\left(\tau_{V_a}\right)\right],\\
\tau_{V_a} &= k_{V_a 1}z_{V_a 1} + z_{V_a 2},\\
\hat{\boldsymbol{\eta}}_{V_a}\left(\tau_{V_a} \mid \hat{\boldsymbol{\zeta}}_{\eta V_a}\right) &= \hat{\boldsymbol{\zeta}}_{\eta V_a}^T \boldsymbol{\varrho}\left(\tau_{V_a}\right),\\
\dot{\hat{\zeta}}_{\eta V_a} &= \gamma_{V_a}\tau_{V_a}\varrho\left(\tau_{V_a}\right).
\end{aligned}
\tag{32}
$$

(i) When f and g are unknown nonlinear functions, the control law, sliding surface, fuzzy system output, and adaptive law can be designed as

$$
\begin{aligned}
U_4 &= \frac{1}{\hat{g}_{V_a}(x_5,t)}\left[-\hat{f}_{V_a}(x_7,t) - k_{V_a 1}z_{V_a 2}\right.\\
&\quad \left. + \ddot{x}_{7\,d} - \hat{\eta}_{V_a}\left(\tau_{V_a}\right)\right],\\
\tau_{V_a} &= k_{V_a 1}z_{V_a 1} + z_{V_a 2},\\
\hat{f}_{V_a}\left(x_7 \mid \boldsymbol{\zeta}_{f_{\Phi V_a}}\right) &= \hat{\boldsymbol{\zeta}}_{f_{V_a}}^T \boldsymbol{\xi}\left(\tau_{V_a}\right),\\
\hat{g}_{V_a}\left(x_7 \mid \boldsymbol{\zeta}_{g_{V_a}}\right) &= \hat{\boldsymbol{\zeta}}_{g_{V_a}}^T \boldsymbol{\xi}\left(\tau_{V_a}\right),\\
\hat{\boldsymbol{\eta}}_{V_a}\left(\tau_{V_a} \mid \hat{\boldsymbol{\zeta}}_{\eta V_a}\right) &= \hat{\boldsymbol{\zeta}}_{\eta V_a}^T \boldsymbol{\varrho}\left(\tau_{V_a}\right),\\
\dot{\hat{\zeta}}_{f_{V_a}} &= \gamma_{1V_a}\tau_{V_a}\xi(x_7),\\
\dot{\hat{\zeta}}_{g_{V_a}} &= \gamma_{2V_a}\tau_{V_a}\xi(x_7)U_2,\\
\dot{\hat{\zeta}}_{\eta V_a} &= \gamma_{V_a}\tau_{V_a}\varrho\left(\tau_{V_a}\right).
\end{aligned}
\tag{33}
$$

3.3. Altitude Controller Design. The flight altitude controller of a fixed-wing UAV is more complicated than the previous two controllers because altitude control is an indirect control process rather than a direct control process.

The mathematical model related to altitude is analyzed at first.

$$
\dot{P}_z = \sin\theta u - \cos\theta \sin\Phi v - \cos\theta\cos\Phi w. \tag{34}
$$

It is acknowledged that the flight height of a fixed-wing UAV is mainly related to the pitch angle and airspeed. Therefore, the above equation can be expressed as follows:

$$
\begin{aligned}
\dot{P}_z &= u\theta + \sin\theta u - u\theta - \cos\theta\sin\Phi v - \cos\theta\cos\Phi w\\
&= u\theta + d_{P_z},
\end{aligned}
\tag{35}
$$

where $d_{P_z} = \sin\theta u - u\theta - \cos\theta\sin\Phi v - \cos\theta\cos\Phi w$ is defined as disturbance.

As can be seen from the above equation, the flight height can be changed by controlling both the airspeed and pitch angle. Therefore, two different coupling controllers were designed in this section. The previously designed adaptive fuzzy sliding mode controllers for pitch angle and airspeed were used as the inner loop of the two controllers. The outer control loop is a traditional PID controller. This is because, in the coupling controller, the performance of PID is often more stable and better than that of other control methods as an outer loop controller.

The controller of flight height assisted by pitch angle is designed as follows.

$$
\dot{P}_z = u\theta + d_{P_z}. \tag{36}
$$

In the design of the controller, the airspeed is a constant value under the ideal state, so it can be regarded as a constant for the further design of the controller. Under this condition, Laplace variation was performed using the above equation:

$$
P_z(s) = \frac{u}{s}\left(\theta + \frac{1}{u}d_{P_z}\right). \tag{37}
$$

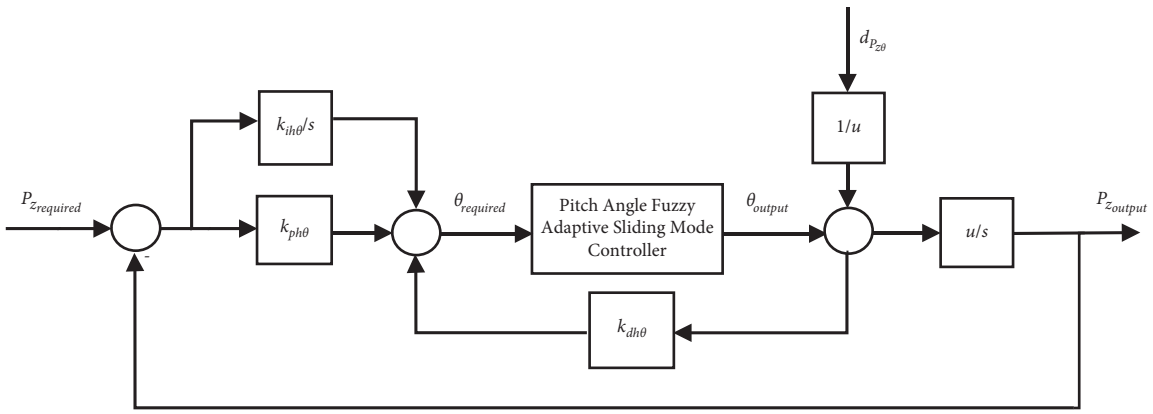

Figure 2: Flight height coupling controller based on pitch angle.

Therefore, the height controller assisted by the pitch angle can be designed, as shown in Figure 2.

First, the target height is the input of the PID control system of the outer loop, and the target pitch angle is obtained after processing by the PID controller. Then, the target pitch angle was used as the input for the fuzzy adaptive sliding mode control of the pitch angle. Subsequently, the output signal of the inner loop is returned to the PID controller of the outer loop to control the flight height.

Similarly, the pitch angle was set to a constant value when the altitude controller assisted by the flight speed was designed.

Laplace variation of equation (36) can be obtained as follows.

$$P_z(s) = \frac{\theta}{s}\left(u + \frac{1}{\theta}d_{P_z}\right). \tag{38}$$

Therefore, the altitude controller assisted by airspeed can be designed as shown in Figure 3.

The outer loop PID control calculates the required airspeed according to the command height. Then, the control process of airspeed is realized through the fuzzy adaptive sliding mode control of the inner loop. After that, the signal is returned to the outer loop controller, and the height is output after introducing the uncertain term.

3.4. Stability Analysis. Stability is the most powerful performance index for determining a controller in a controlled system. Because the controller design idea is similar, the yaw angle controllers are taken as an example to analyze the stability of the controllers under both known f and g and unknown f and g conditions.

First, the stability of the yaw angle fuzzy adaptive sliding mode controller is analyzed under the condition of known f and g.

Define the optimal parameter as

$$\zeta_\eta^* = \arg\min_{\hat{\zeta}_\eta \in \Omega_\eta}\left[\sup\left|\hat{\eta}_\Psi\left(\tau_\Psi|\hat{\zeta}_\eta\right) - \eta_\Psi \mathrm{sgn}(\tau_\Psi)\right|\right], \tag{39}$$

where Ω_η is the set of $\hat{\zeta}_\eta$.

Substitute the control law equation (20) to obtain

$$\begin{aligned}
\dot{\tau}_\Psi &= k_{\Psi 1}\dot{z}_{\Psi 1} + \ddot{x}_1 - \ddot{x}_{1\,d} \\
&= k_{\Psi 1}\dot{z}_{\Psi 1} + \dot{x}_2 - \ddot{x}_{1\,d} \\
&= k_{\Psi 1} z_{\Psi 1} + f(x_1, t) + g(x_1, t)U_2 + d_\Psi - \ddot{x}_d \\
&= -\hat{\eta}_\Psi\left(\tau_\Psi|\hat{\zeta}_\eta\right) + d_\Psi - \hat{\eta}_\Psi\left(\tau_\Psi|\hat{\zeta}_\eta\right) \\
&\quad + d_\Psi + \hat{\eta}_\Psi\left(\tau_\Psi|\zeta_\eta^*\right) - \hat{\eta}_\Psi\left(\tau_\Psi|\zeta_\eta^*\right) \\
&= \tilde{\zeta}_\eta^T \varrho(\tau_\Psi) + d_\Psi - \hat{\eta}_\Psi\left(\tau_\Psi|\zeta_\eta^*\right),
\end{aligned} \tag{40}$$

where $\tilde{\zeta}_\eta = \zeta_\eta^* - \hat{\zeta}_\eta$.

Establish the Lyapunov function as

$$V_\Psi = \frac{1}{2}\left(\tau_\Psi{}^2 + \frac{1}{\gamma}\tilde{\zeta}_\eta^T\tilde{\zeta}_\eta\right). \tag{41}$$

Take the derivative of it to get

$$\begin{aligned}
\dot{V}_\Psi &= \tau_\Psi\dot{\tau}_\Psi + \frac{1}{\gamma}\tilde{\zeta}_\eta^T\dot{\tilde{\zeta}}_\eta \\
&= \tau_\Psi\left(\tilde{\zeta}_\eta^T\varrho(\tau_\Psi) + d_\Psi - \hat{\eta}_\Psi\left(\tau_\Psi|\zeta_\eta^*\right)\right) + \frac{1}{\gamma}\tilde{\zeta}_\eta^T\dot{\tilde{\zeta}}_\eta \\
&= \tau_\Psi\tilde{\zeta}_\eta^T\varrho(\tau_\Psi) + \frac{1}{\gamma}\tilde{\zeta}_\eta^T\dot{\tilde{\zeta}}_\eta + \tau_\Psi\left(d_\Psi - \hat{\eta}_\Psi\left(\tau_\Psi|\zeta_\eta^*\right)\right).
\end{aligned} \tag{42}$$

Substitute $\hat{\eta}_\Psi(\tau_\Psi|\zeta_\eta^*) = \eta_\Psi \mathrm{sgn}(\tau_\Psi)$ into the above equation.

$$\dot{V}_\Psi = \frac{1}{\gamma}\tilde{\zeta}_\eta^T\left(\gamma\tau_\Psi\varrho(\tau_\Psi) - \dot{\hat{\zeta}}_\eta\right) + \tau_\Psi d_\Psi - \eta_\Psi|\tau_\Psi|, \tag{43}$$

where $\dot{\tilde{\zeta}}_\eta = -\dot{\hat{\zeta}}_\eta$.

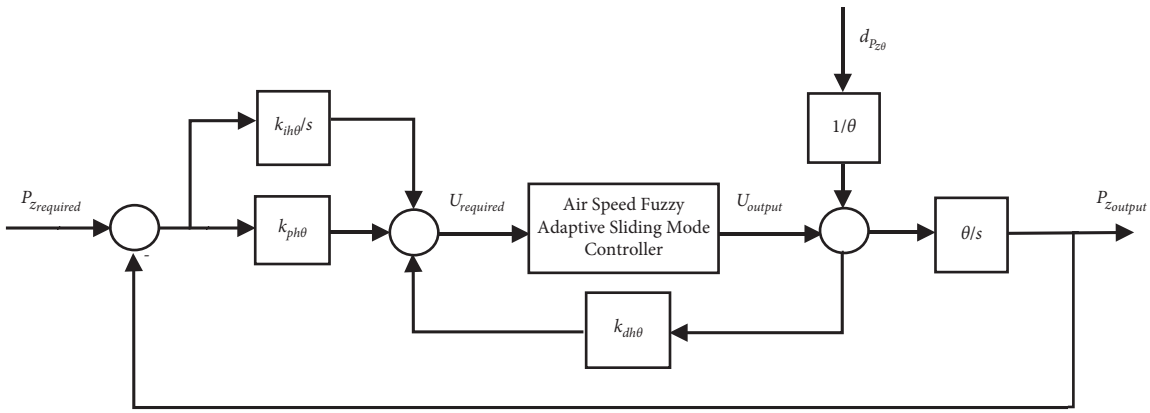

Figure 3: Flight height coupled controller based on airspeed.

Substitute the adaptive law to obtain

$$\dot{V}_\Psi = \tau_\Psi d_\Psi - \eta_\Psi |\tau_\Psi|. \tag{44}$$

Take $\eta_\Psi = \eta_{\Psi 0} + D$, $\eta_{\Psi 0} > 0$.

Therefore, $\dot{V}_\Psi \le -\eta_{\Psi 0}|\tau_\Psi| \le 0$.

When $\dot{V}_\Psi \equiv 0$, $\tau_\Psi \equiv 0$. According to LaSalle invariant set principle, when $t \longrightarrow \infty$, $\tau_\Psi \longrightarrow 0$, $z_{\Psi 1} \longrightarrow 0$.

The stability of the system can be obtained based on Lyapunov's second law [30].

Second, the stability of the fuzzy adaptive sliding mode controller was analyzed in the case of unknown f and g.

Define the optimal parameter as

$$\begin{aligned}
\zeta_f^* &= \arg_{\hat{\zeta}_f \in \Omega_f} \min\left[\sup\left|\hat{f}\left(\tau_\Psi \mid \hat{\zeta}_f\right) - f(x_1,t)\right|\right],\\
\zeta_g^* &= \arg_{\hat{\zeta}_g \in \Omega_g} \min\left[\sup\left|\hat{g}\left(\tau_\Psi \mid \hat{\zeta}_g\right) - g(x_1,t)\right|\right],\\
\zeta_\eta^* &= \arg_{\hat{\zeta}_\eta \in \Omega_\eta} \min\left[\sup\left|\hat{\eta}_\Psi\left(\tau_\Psi \mid \hat{\zeta}_\eta\right) - \eta_\Psi \mathrm{sgn}(\tau_\Psi)\right|\right],
\end{aligned} \tag{45}$$

where Ω_f, Ω_g, and Ω_η are the sets of $\hat{\zeta}_f$, $\hat{\zeta}_g$, and $\hat{\zeta}_\eta$.

Define the minimum approximation error $\omega_\Psi = f(x_1,t) - \hat{f}_\Psi(\tau_\Psi \mid \zeta_f^*) + (g(x_1,t) - \hat{g}_\Psi(\tau_\Psi \mid \zeta_g^*))U_2$, $|\omega_\Psi| \le \omega_{\max}$.

$$\begin{aligned}
\dot{\bar{u}}_\Psi &= K_{\Psi 1}\dot{z}_{\psi 1} + \ddot{x} - \ddot{x}_{1\,d}\\
&= K_{\Psi 1}\dot{z}_{\Psi 1} + \ddot{x}_2 - \ddot{x}_{1\,d}\\
&= K_{\Psi 1}\dot{z}_{\Psi 1} + f(x_1,t) + g(x_1,t)U_2 + b\left(\hat{g}_\Psi(x_1,t) - \hat{g}_\Psi(x_1,t)\right)U_2 + d_\Psi - \ddot{x}_d\\
&= K_{\Psi 1}\dot{z}_{\Psi 1} + f(x_1,t) + g(x_1,t)U_2 + \left(g_\Psi(x_1,t) - \hat{g}_\Psi(x_1,t)\right)U_2 + d_\Psi - \ddot{x}_d\\
&= \hat{f}(x_1,t) - \eta_\Psi\left(\tau_\Psi|\hat{\zeta}_\eta\right) + \left(g_\psi(x_1,t) - \hat{g}_\psi(x_1,t)\right)U_2 + d_\Psi - \ddot{x}_d\\
&= \hat{f}_\Psi\left(x_1|\hat{\zeta}_f\right) - \hat{f}(x_1,t) - \hat{\eta}_\Psi\left(\tau_\Psi|\hat{\zeta}_\eta\right) + \left(\hat{g}_\psi\left(x_1|\hat{\zeta}_g^*\right) - \hat{g}_\psi(x_1,t)\right)U_2 + d_\Psi + \omega_\Psi + \hat{\eta}_\Psi\left(\tau_\Psi|\hat{\zeta}_\eta^*\right) - \hat{\eta}_\psi\left(\tau_\Psi|\hat{\zeta}_\eta^*\right)\\
&= \tilde{\zeta}_f^T\xi(x_1) + \tilde{\zeta}_g^T\xi(x_1)U_2 + \tilde{\zeta}_g^T\varsigma(\tau_\Psi) + d_\Psi + \omega_\Psi - \hat{\eta}_\Psi\left(\tau_\Psi|\hat{\zeta}_\eta^*\right).
\end{aligned} \tag{46}$$

Substitute the control law (equation 23): $\tilde{\zeta}_f = \zeta_f^* - \hat{\zeta}_f$, $\tilde{\zeta}_g = \zeta_g^* - \zeta_g$, $\tilde{\zeta}_\eta = \zeta_\eta^* - \zeta_\eta$.

Define the Lyapunov equation:

$$V_\Psi = \frac{1}{2}\left(\tau_\Psi{}^2 + \frac{1}{\gamma_{1\Psi}}\tilde{\zeta}_f^T\tilde{\zeta}_f + \frac{1}{\gamma_{2\Psi}}\tilde{\zeta}_g^T\tilde{\zeta}_g + \frac{1}{\gamma_\Psi}\tilde{\zeta}_\eta^T\tilde{\zeta}_\eta\right), \tag{47}$$

where $\gamma_{1\Psi} > 0$, $\gamma_{2\Psi} > 0$, and $\gamma_\Psi > 0$.

The derivative of the above equation is

$$\begin{aligned}\dot{V}_\Psi &= \tau_\Psi \dot{\tau}_\Psi + \frac{1}{\gamma_1}\tilde{\zeta}_f^T\dot{\tilde{\zeta}}_f + \frac{1}{\gamma_2}\tilde{\zeta}_g^T\dot{\tilde{\zeta}}_g + \frac{1}{\gamma}\tilde{\zeta}_\eta^T\dot{\tilde{\zeta}}_\eta \\ &= \tau_\Psi\left(\tilde{\zeta}_f^T\xi(x_1) + \tilde{\zeta}_g^T\xi(x_1)U_2 + \tilde{\zeta}_\eta^T\varrho(\tau_\Psi) + \omega_\Psi + d_\Psi - \hat{\eta}_\Psi\left(\tau_\Psi|\zeta_\eta^*\right)\right) + \frac{1}{\gamma_1}\tilde{\zeta}_f^T\dot{\tilde{\zeta}}_f + \frac{1}{\gamma_2}\tilde{\zeta}_g^T\dot{\tilde{\zeta}}_g + \frac{1}{\gamma}\tilde{\zeta}_\eta^T\dot{\tilde{\zeta}}_\eta \\ &= \tau_\Psi\tilde{\zeta}_f^T\xi(x_1) + \frac{1}{\gamma_1}\tilde{\zeta}_f^T\dot{\tilde{\zeta}}_f + \tau_\Psi\tilde{\zeta}_g^T\xi(x_1) + \tau_\Psi\tilde{\zeta}_\eta^T\varrho(\tau_\Psi) + \frac{1}{\gamma}\tilde{\zeta}_\eta^T *_\eta + \tau_\Psi\left(d_\Psi - \hat{\eta}_\Psi\left(\tau_\Psi|\zeta_\eta^*\right)\right).\end{aligned} \tag{48}$$

Substitute $\hat{\eta}_\Psi(\tau_\Psi|\zeta_\eta^*) = \eta_\Psi \mathrm{sgn}(\tau_\Psi)$ into the above equation:

$$\begin{aligned}\dot{V}_\Psi &= \frac{1}{\gamma_1}\tilde{\zeta}_f^T\left(\gamma_1\tau_\Psi\xi(x_1) + \dot{\tilde{\zeta}}_f\right) + \frac{1}{\gamma_2}\left(\gamma_2\tau_\Psi\xi(x_1)U_2 + \dot{\tilde{\zeta}}_g\right) + \frac{1}{\gamma}\left(\gamma\tau_\Psi\eta_{\eta\Psi}^T\varrho(\tau_\Psi) + \dot{\tilde{\zeta}}_\eta\right) + \tau_\Psi d_\Psi + \tau_\Psi\omega_\Psi - (D+\eta)|\tau_\Psi| \\ &= \tau_\Psi d_\Psi + \tau_\Psi\omega_\Psi - (D+\eta_\Psi)|s|,\end{aligned} \tag{49}$$

where $\dot{\tilde{\zeta}}_f = -\dot{\tilde{\zeta}}_f$, $\dot{\tilde{\zeta}}_g = -\dot{\tilde{\zeta}}_g$, $\dot{\tilde{\zeta}}_\eta = -\dot{\tilde{\zeta}}_\eta$.

Substitute the adaptive law into the above equation:

$$\dot{V}_\Psi \le \tau_\Psi\omega_\Psi - \eta_\Psi|\tau_\Psi|. \tag{50}$$

According to the fuzzy approximation theory, the adaptive fuzzy system can realize a minimum approximation error. By taking η_Ψ big enough, $\eta_\Psi = \eta_{0\Psi} + |\omega_\Psi|_{\max}$, $\eta_{0\Psi} > 0$, so $\dot{V}_\Psi \le -\eta_{0\Psi}|\tau_\Psi| \le 0$.

When $\dot{V}_\Psi \equiv 0$, $\tau_\Psi \equiv 0$. According to LaSalle invariant set principle, when $t \longrightarrow \infty$, $\tau_\Psi \longrightarrow 0$, $z_{\Psi 1} \longrightarrow 0$.

Similarly, according to Lyapunov's second law, the stability of the system can be obtained.

The other controllers, similar to the yaw angle controllers, can also be proven to be stable.

4. Simulation of the Control Process

In the fourth section, the simulation results of designed controllers are provided.

To fully compare the superior performance of fuzzy adaptive sliding mode control, the simulation results of the traditional sliding mode controller are also included in this section.

A fixed-wing UAV is a deeply coupled system in the working process. Any change in one state variable will affect the other state variables, so all controllers work synchronously.

However, in order to show the performance details of each controller, this section is divided into three parts, and the simulation comparison results of the attitude controller, airspeed controller, and height controller are analyzed in detail. For each variable, the related complex fuzzy adaptive sliding mode controller, simple fuzzy adaptive sliding mode controller based on switching items only, and traditional sliding mode controller are simulated and compared.

4.1. Posture Simulation. Before the simulation, the membership function of the fuzzy items in the designed control algorithm should be selected first. In fuzzy control, membership functions are mainly used to approximate unknown terms, while the selection method of these functions is not an easy task. The selection of membership functions directly determines whether the fuzzy algorithm can show the ideal performance. At present, the selection method of membership functions for fuzzy control is mainly determined by experience.

In this study, a lot of relevant literatures have been referred, and a large number of simulations have been tested to find the appropriate membership functions that can help the controller achieve the control effect.

In the attitude angle control simulation, five membership functions in the comprehensive fuzzy adaptive sliding mode controller are used for the fuzzification of f and g:

(i) $\mu_{\mathrm{NM}}(x_i) = \exp[-(((x_i+\pi)/3)/(\pi/12))^2]$

(ii) $\mu_{\mathrm{NS}}(x_i) = \exp[-(((x_i+\pi)/6)/(\pi/12))^2]$

(iii) $\mu_Z(x_i) = \exp[-(x_i/(\pi/12))^2]$

(iv) $\mu_{\mathrm{PS}}(x_i) = \exp[-(((x_i-\pi)/6/((\pi/12)))^2]$

(v) $\mu_{\mathrm{PM}}(x_i) = \exp[-(((x_i-\pi)/3)/(\pi/12))^2]$

As shown in Figure 4, there are 25 fuzzy rules for approximating f and g, respectively.

The same membership functions are selected for the switching items in the complex fuzzy sliding mode controller and fuzzy sliding mode controller based on the switching item only. The membership functions of the switching item are defined as follows:

(i) $\mu_{\mathrm{NS}}(s) = 1/(1+\exp(8(s+4)))$

(ii) $\mu_{\mathrm{NZ}}(s) = \exp(-s^2)$

(iii) $\mu_{\mathrm{NP}}(s) = 1/(1+\exp(8(s-4)))$

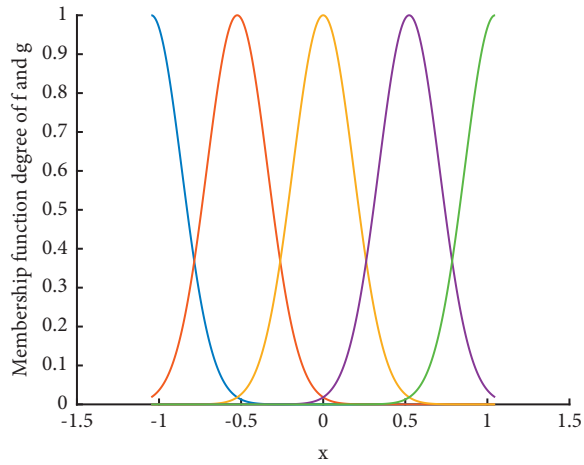

Figure 4: Fuzzy rules for f and g.

As shown in Figure 5, there 3 fuzzy rules for approximating switch item.

Furthermore, the selection of adaptive parameters is also not an easy task. Appropriate adaptive parameters can help the adaptive fuzzy sliding mode control system to reach the sliding mode surface gradually and stably. Therefore, it is significant to take appropriate value of adaptive terms. However, there is no convenient method to select adaptive parameters. In this study, the more suitable adaptive parameters are obtained through many experiments in simulation.

In practice, attitude control is usually achieved at an angle and then maintained. In order to better demonstrate the superior performance of the controller tracking, the command signals are assumed to be sinusoidal signals in the simulation $(0.5\sin(t), 0.5\sin(t), 0.5\sin(t))$. The initial attitude angles were set to $(0, 0, 0)$. The initial values of airspeed and flight altitude in the attitude angle control simulation were set to 50 m/s and 2500 m, respectively.

First, the simulation results of yaw angle are analyzed.

The control parameters of yaw angle controllers are selected as follows:

(i) Comprehensive fuzzy adaptive sliding mode controller: $k_{\Psi 1} = 5$, $\gamma_{1\Psi} = 7$, $\gamma_{2\Psi} = 2$, $\gamma_{\Psi} = 6$

(ii) Fuzzy adaptive sliding mode controller based on switching item only: $k_{\Psi 1} = 29$, $\gamma_{\Psi} = 140$

(iii) Traditional sliding mode control law:

$$U_2 = \frac{1}{g_{\Psi}(x_1, t)}\left[-f_{\Psi}(x_1, t) - k_{\Psi 1} z_{\Psi 2} + \ddot{x}_{1\,d} - c_{\Psi}\dot{z}_{\Psi 1} - \ell_{\Psi}\mathrm{sgn}(\tau_{\Psi})\right] - d_{\Psi}\mathrm{sgn}(\tau_{\Psi}), \tag{51}$$

where $k_{\Psi} = 9$, $c_{\Psi} = 7$, and $\ell_{\Psi} = 13$.

The uncertainty is taken as $d_{\Psi} = 13\sin(t)$.

The following simulation results can be obtained, as given in Table 3 and Figure 6.

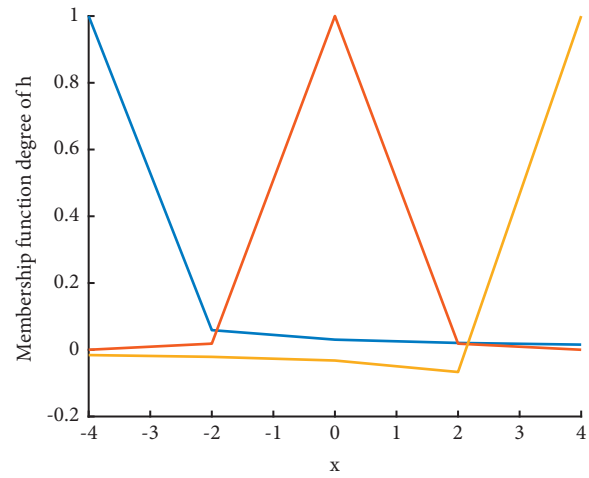

Figure 5: Fuzzy rules for switch item.

Table 3: Yaw angle controller performance indexes.

Items	SM	FSM without f and g	FSM with f and g
Reaction time (s)	0.201	0.214	0.215
Error (0.01 rad)	0.1	−0.07	0.37
Overshoot (0.01 rad)	0.12	0	0.4

Table 3 provides several performance indexes of three controllers. These performance indicators include reaction time (the time of track signal's first reach at 0.1 rad), end point error (the error of the tracking signal when the command signal reaches the first peak), and overshoot (the maximum overshoot of the tracking signal before the first downtrend of the command signal). Figures 6(a) and 6(d) and Table 3 show the simulation result of the yaw angle tracking. It can be seen from Figure 6(a) that the three controllers can complete the yaw angle control process well generally. Figure 6(d) is a partial enlargement of Figure 6(a)

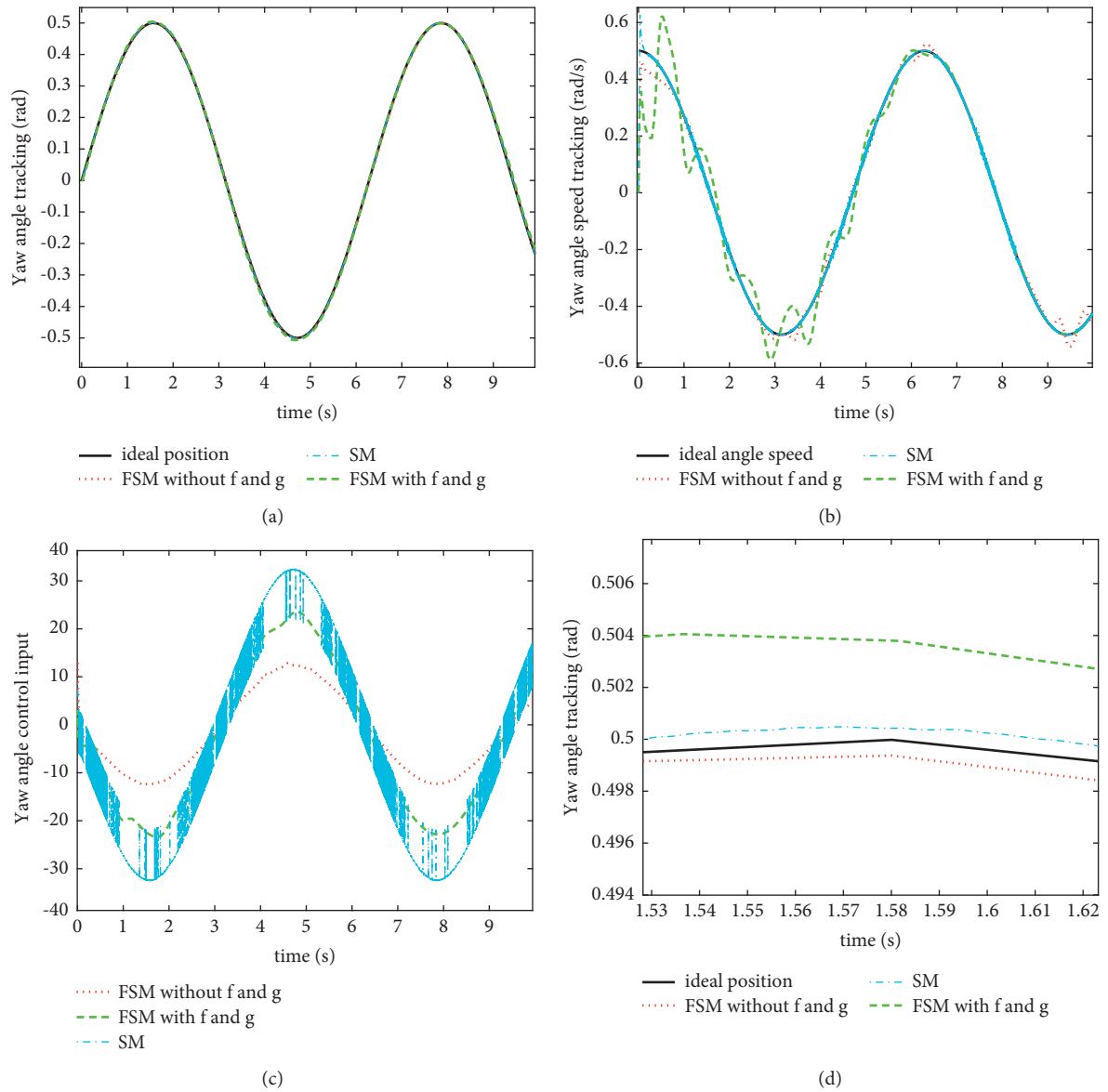

FIGURE 6: Yaw angle-related signal comparison. (a) Yaw angle tracking comparison. (b) Yaw angle speed tracking comparison. (c) Yaw angle control input signal comparison. (d) Partial enlargement of Figure 6(a) at the first peak value.

at the first peak value, from which we can see the differences in details of the control effects of the three controllers. As can be seen from figure and Table 3, when the instruction signal reaches the first peak value, FSM with f and g has the largest error and overshoot, while FSM without f and g has the smallest error and no overshoot. Moreover, the traditional sliding mode controller has the fastest response speed. This is mainly because when the fuzzy adaptive processing of the switching term eliminates the chattering phenomenon, it will also reduce the reaction speed slightly, but the influence is not significant and can be ignored. Figure 6(b) shows the tracking situation of the angle change speed of the three controllers in the yaw angle control process. Among them, the fuzzy adaptive sliding mode controller only for switching items (FSM with f and g) has the worst performance, and jitter occurs many times during the tracking process. The best performance is that of the traditional sliding mode controller (SM). There was only a small deviation in the initial stages. The deviation of the fuzzy adaptive sliding mode controller (FSM without f and g) also exists, but the degree is small. Figure 6(c) shows the control input signal. Obviously, the best performance is the comprehensive fuzzy adaptive sliding mode controller because its amplitude is smaller and more stable than the other two terms. For a controller, a smaller amplitude can contribute to ensuring the stability of the system and the working life of the controller. The amplitude of the fuzzy adaptive sliding mode controller based only on the switching item is larger than that of the former, and the performance is slightly worse. On the other hand, the traditional sliding mode controller has continuous vibration of its control input signal, which is called shaking. This is not the case in the other two

controllers, mainly because the adaptive fuzzy method is used to handle the switching items. It can be seen that the introduction of the fuzzy adaptive method to the sliding mode control can effectively eliminate shaking.

Second, the simulation results of the pitch angle controller are analyzed.

The control parameters of pitch angle controllers are selected as follows:

(i) Comprehensive fuzzy adaptive sliding mode controller: $k_{\theta 1} = 4$; $\gamma_{1\theta} = 6$; $\gamma_{2\theta} = 3$; $\gamma_{\theta} = 5$

(ii) Fuzzy adaptive sliding mode controller based on switching item only: $k_{\theta 1} = 31$; $\gamma_{\theta} = 150$

(iii) Traditional sliding mode control law is designed as

$$U_1 = \frac{1}{g_\theta(x_3,t)}\left[-f_\theta(x_3,t) - k_{\theta 1}z_{\theta 2} + \ddot{x}_{3\,d} - c_\theta \dot{z}_{\theta 1} - \ell_\theta \operatorname{sgn}(\tau_\theta)\right] - d_\theta \operatorname{sgn}(\tau_\theta), \tag{52}$$

where $k_\theta = 11$, $c_\theta = 9$, and $\ell_\theta = 15$.

The related uncertainty is taken as $d_\theta = 13\sin(t)$.

Figure 7(a) shows the simulation outputs of the pitch angle controllers. Similar to the yaw angle control, the outputs of the three controllers are almost equally superior generally. It can be seen from Figure 7(d) and Table 4 that FSM with f and g deviates most from the command signal and own the max error and overshoot. Moreover, the performance of traditional sliding mode control and FSM without f and g are similar to the command signal, but the traditional sliding mode control slightly exceeds the command signal, while the latter is always lower than the command signal. In addition, the traditional sliding mode control still has the fastest response speed, which is consistent with the yaw angle simulation. Figure 7(b) shows the change rate of the pitch angle during the control process. Similarly, the fluctuation of the traditional sliding mode control is the smallest, and the deviation of the fuzzy adaptive sliding mode control based only on switching terms is the most serious. As shown in Figure 7(c), the control input signal of the total fuzzy adaptive sliding mode control still exhibits the best performance. Although the vibration amplitude of the traditional sliding mode control in pitch angle control is smaller than that in yaw angle control, it persists.

Finally, the simulation results of roll angle are analyzed.

The control parameters of roll angle controllers are selected as follows:

(i) Comprehensive fuzzy adaptive sliding mode controller: $k_{\Phi 1} = 7$, $\gamma_{1\Phi} = 9$, $\gamma_{2\Phi} = 1$, $\gamma_{\Phi} = 8$

(ii) Fuzzy adaptive sliding mode controller based on switching item only: $k_{\Phi 1} = 35$, $\gamma_{\Phi} = 130$

(iii) Traditional sliding mode control law:

$$U_4 = \frac{1}{g_{V_a}(x_5,t)}\left[-f_{V_a}(x_5,t) - k_{\Phi 1}z_{\Phi 2} + \ddot{x}_{5\,d} - c_\Phi \dot{z}_{\Phi 1} - \ell_\Phi \operatorname{sgn}(\tau_\Phi)\right] - d_\Phi \operatorname{sgn}(\tau_\Phi), \tag{53}$$

where $k_\Phi = 13$, $c_\Phi = 7$, and $\ell_\Phi = 12$.

The related uncertainty is taken as $d_\Phi = 15\sin(t)$.

Figure 8(a) shows the output simulation results for the roll angle controller. The output of the controller is similar to that described above (Figure 7(a)). According to the information recorded in Figure 8(d) and Table 5, the reaction speed is the same as the above situation, whereas the traditional sliding mode control has the minimum error and overshoot when the first peak arrives. Moreover, in the first peak stage, FSM without F and G showed obvious lag and unsatisfactory performance, while the traditional sliding mode control is the most suitable control signal curve. Only from the tracking of roll angle, the traditional sliding mode control seem shows the best control performance.

In the case of the speed change of the roll angle, the fuzzy adaptive sliding mode controller based only on switching terms has the best performance, which almost closely fits the ideal speed change curve (Figure 8(b)). As shown in Figure 8(c), in the control process of the roll angle, the amplitude of the input signal of the comprehensive fuzzy adaptive sliding mode controller and the fuzzy adaptive sliding mode controller only for switching item are close to each other. The shaking of the traditional sliding mode controller is very serious. Considering the above, FSM with f and g seem own the best performing. However, FSM without f and g only shows slight lag phenomenon when f and g are uncertain, and other performance is similar to the former, so the latter is still a better choice in practical application.

In general, in the simulation process of the attitude angle, the control effects of each controller are close, and the control process can be completed quickly with less error. The traditional sliding mode control has continuous shaking, but the fuzzy adaptive method can solve this problem. The comprehensive performance of the fuzzy adaptive sliding mode controller is the best because the amplitude of the control input signal is the smallest, and the controller does not need to design the switching term, f function, and g function accurately in advance.

4.2. Airspeed Simulation. In the airspeed simulation, the initial state of the attitude angle is (0, 0, 0), and the flight altitude is 2500 m. The starting airspeed was 30 m/s, and the target airspeed was 50 m/s.

The membership functions for f_{V_a} and g_{V_a} are taken as follows.

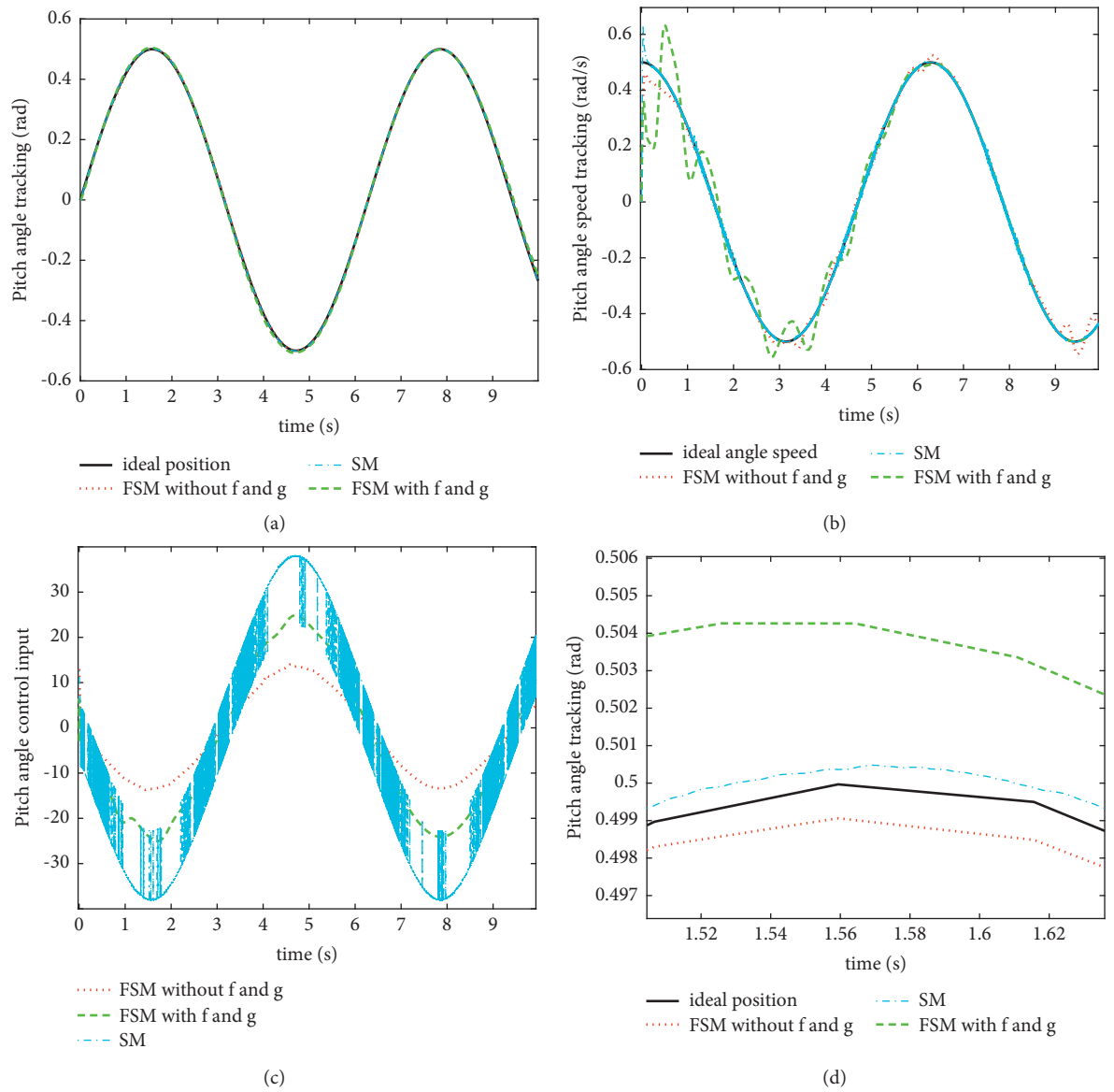

Figure 7: Pitch angle related signal comparison. (a) Pitch angle tracking comparison. (b) Pitch angle speed tracking comparison. (c) Pitch angle control input signal comparison. (d) Partial enlargement of Figure 7(a) at the first peak value.

Table 4: Pitch angle controller performance indexes.

Items	SM	FSM without f and g	FSM with f and g
Reaction time (s)	0.211	0.232	0.234
Error (0.01 rad)	0.05	−0.12	0.41
Overshoot (0.01 rad)	0.09	0	0.43

(i) $\mu_{\mathrm{NM}}(x_i) = \exp[-(((x_i + \pi)/6)/(\pi/24))^2]$

(ii) $\mu_{\mathrm{NS}}(x_i) = \exp[-(((x_i + \pi)/6)/(\pi/24))^2]$

(iii) $\mu_Z(x_i) = \exp[-(x_i/(\pi/24))^2]$

(iv) $\mu_{\mathrm{PS}}(x_i) = \exp[-(((x_i - \pi)/6)/(\pi/24))^2]$

(v) $\mu_{\mathrm{PM}}(x_i) = \exp[-(((x_i - \pi)/6)/(\pi/24))^2]$

The membership functions of the switching item are taken as follows.

(i) $\mu_N(s) = 1/(1 + \exp(12(s + 6)))$

(ii) $\mu_N(s) = \exp(-s^2)$

(iii) $\mu_N(s) = 1/(1 + \exp(12(s - 6)))$

The parameters for each controller are selected as follows:

(i) Comprehensive fuzzy adaptive sliding mode controller: $k_{V_a}1 = 21$, $\gamma_{1V_a} = 17$, $\gamma_{2V_a} = 5$, $\gamma_{V_a} = 13$.

(ii) Fuzzy adaptive sliding mode controller based on switching item only: $k_{V_a}1 = 50$, $\gamma_{V_a} = 190$.

(iii) Traditional sliding mode control law:

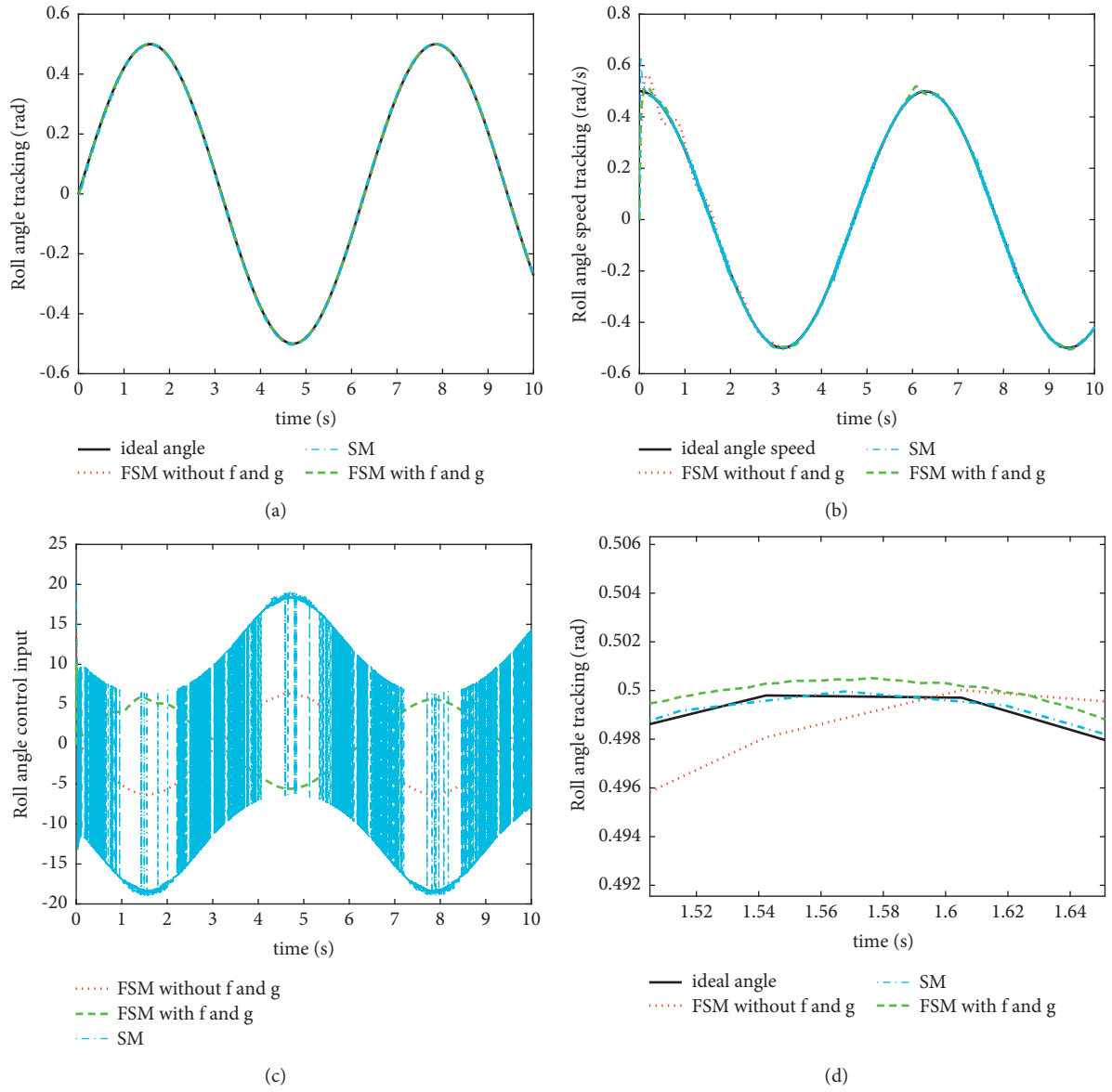

Figure 8: Roll angle related signal comparison. (a) Roll angle tracking comparison. (b) Roll angle speed tracking comparison. (c) Roll angle control input signal comparison. (d) Partial enlargement of Figure 8(a) at the first peak value.

Table 5: Roll angle controller performance indexes.

Items	SM	FSM without f and g	FSM with f and g
Reaction time (s)	0.198	0.219	0.221
Error (0.01 rad)	−0.03	−0.32	0.19
Overshoot (0.01 rad)	0.01	0.35	0.39

$$U_4 = \frac{1}{g_{V_a}(x_7,t)}\left[-f_{V_a}(x_7,t) - k_{V_a1}z_{V_a2} + \ddot{x}_{7\,d} - c_{V_a}\dot{z}_{V_a1} - \ell_{V_a}\mathrm{sgn}\left(\tau_{V_a}\right)\right] - d_{V_a}\mathrm{sgn}\left(\tau_{V_a}\right) \tag{54}$$

where $k_{V_a} = 24$, $c_{V_a} = 11$, $\ell_{V_a} = 10$.

The related uncertainty is taken as $d_{V_a} = 10\sin(t)$.

Table 6 and Figure 9(a) show the output performance of the three controllers in the airspeed control process. The fuzzy adaptive sliding mode controller only for switching items has serious overshooting (7 m/s), and the response speed is slower than that of the other two controllers. Traditional sliding mode control has the best performance with the fastest response speed and no overshooting or steady-state error. The overall fuzzy adaptive sliding mode control also has no steady-state error, but the response speed is slower than that of the traditional sliding mode control. It can be seen from Figure 9(b) that the shaking problem of the traditional sliding mode control has a phased impact on the tracking performance of the control speed. As shown in Figure 9(c), shaking is still serious in the traditional sliding mode controller, and the comprehensive fuzzy adaptive

Table 6: Airspeed controller performance indexes.

Items	SM	FSM without f and g	FSM with f and g
Steady time (s)	0.35	1.1	3.2
Steady error (m/s)	−0.03	−0.02	0.15
Overshoot (m/s)	0	0	7.2

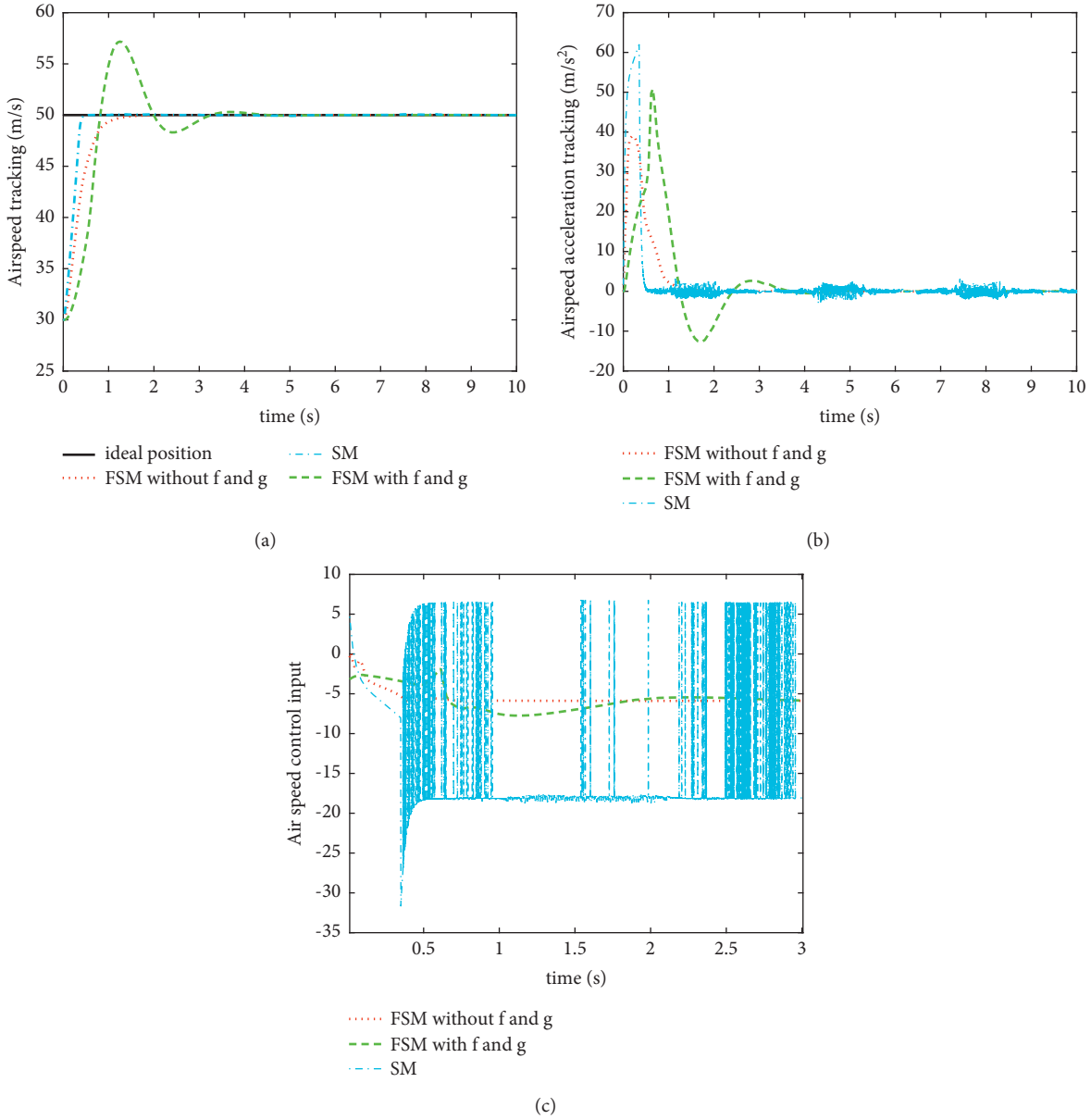

Figure 9: Air speed related signal comparison. (a) Air speed tracking comparison. (b) Air speed change tracking comparison. (c) Air speed control input signal comparison.

sliding mode control tends to stabilize soon after the control process, while the other two controllers do not. Similarly, the total fuzzy adaptive sliding mode control still exhibited a minimum amplitude change.

The biggest difference between altitude control and attitude control is that the altitude control process gap between the command signal and the original state is larger. In this case, the advantages of the traditional sliding mode control are slightly obvious only from the control effect. However, the shaking of the traditional sliding mode controller further affects its tracking speed. It is impossible to guarantee that the control effect of long time and high

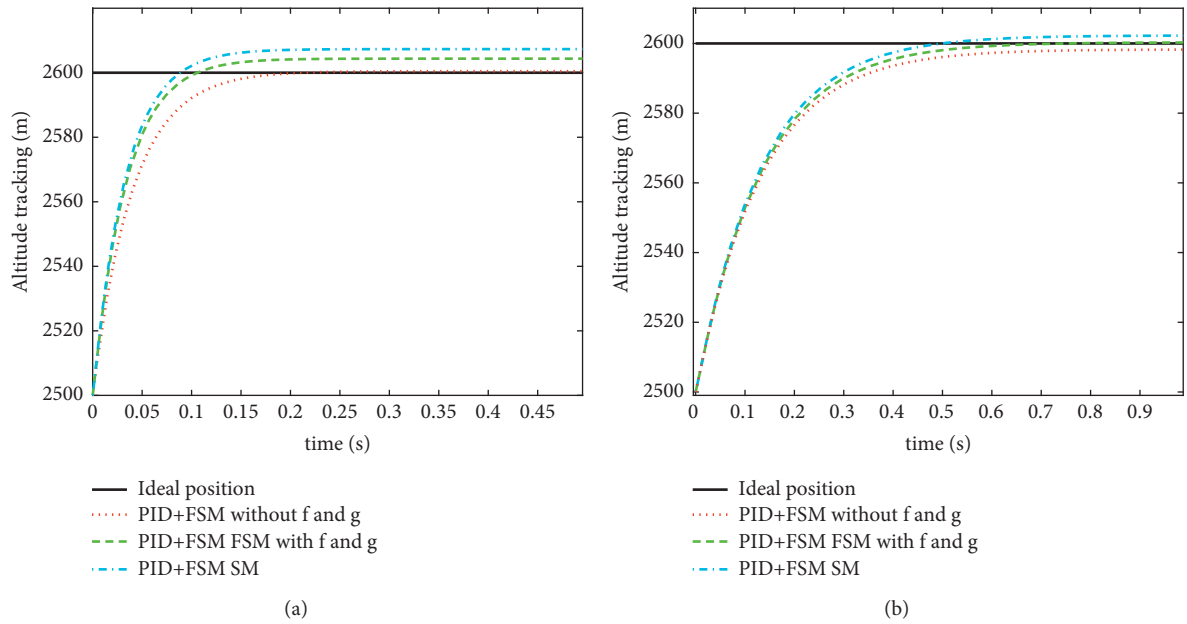

Figure 10: Air speed related signal comparison. (a) Flight altitude controlled by the pitch angle. (b) Flight altitude controlled by the airspeed.

Table 7: Flight altitude controller performance indexes.

Methods	By the pitch angle			By the airspeed		
Items	PID + SM	PID + FSM without f and g	PID + FSM with f and g	PID + SM	PID + FSM without f and g	PID + FSM with f and g
Steady time (s)	0.19	0.17	0.15	0.57	0.61	0.59
Steady error (m)	9.8	0.2	6.1	2.5	-2.2	0.1

frequency will not be affected by shaking; thus, the stability of the traditional sliding mode controller has some hidden dangers.

In general, when there is a large gap between the command signal and the initial state, even if the response speed of the comprehensive fuzzy adaptive sliding mode control is slow, the control input amplitude is lower and the process of returning to the stable state is faster, which, in turn, can ensure the stability of the system. Therefore, a comprehensive fuzzy adaptive sliding mode controller still exhibits the best performance in terms of airspeed control.

4.3. Altitude Simulation. In the flight altitude simulation, the simulation results of coupling the three controllers mentioned above with the PID controller were compared. There are two methods to control the flight altitude: one is led by the flight speed and the other is by the pitch angle. In this section, both altitude control methods are simulated.

The selection of PID control parameters is realized by MATLAB self-adjustment function.

When the pitch angle is used to control the flight altitude simulation, the initial attitude angle is (0, 0, 0) and the airspeed is a fixed value of 30m/s.

Figure 10(a) and Table 7 shows the simulation results for the flight altitude controlled by the pitch angle. All three coupling controllers can realize the height control process, but the PID and simple fuzzy adaptive sliding mode controller (only for switching item) show a steady-state error of approximately 10 m. A similar situation also exists in the PID traditional sliding mode coupling controller. The controller coupled with the PID and total fuzzy adaptive sliding mode controller has the slowest response time, but its control result is the most accurate.

In flight altitude simulation using airspeed control, the pitch angle is set to a fixed value of 0.1 rad, the roll angle and attitude angle are both 0 rad, and the initial airspeed is 30m/s. Figure 10(b) and Table 7 show the simulation results for the flight altitude controlled by the airspeed. The PID-fuzzy simple adaptive sliding mode control (only for switching item) coupling controller exhibits the best performance, whereas the other two controllers have various degrees of steady-state errors.

Comparing the two control methods, the flight altitude control method by airspeed requires a long response time. It takes almost 0.6 s for the controller to complete height control. It takes only approximately 0.15 s to control the flight height by pitch angle. This is mainly because the pitch angle plays a more decisive role in altitude control than the airspeed. However, for different control methods, the mean steady-state error is smaller in the flight altitude control method by airspeed.

In conclusion, when there is a large gap between the altitude command and the UAV altitude state, the altitude adjustment method based on the pitch angle should be selected to achieve a fast response. When the difference between the altitude command and the UAV altitude state is small, it is a better choice to control the flight altitude through the airspeed for less error.

The simulation comparison results in this chapter confirm that the two control methods introduced can basically complete the control of a fixed-wing UAV. However, in practical application, it is difficult to obtain the accurate mathematical model of a fixed-wing UAV. There is also the case of approximation in the modeling process mentioned in chapter 2. Inaccurate modeling will directly affect the performance of "fuzzy adaptive sliding mode control only for switching terms." Therefore, the implementation of this method is relatively complex. On the other hand, the comprehensive fuzzy adaptive sliding mode control method has no high requirement for accurate model building and is easier to implement in practical application.

5. Conclusion

A fixed-wing UAV is a complex, nonlinear, multivariable, and strongly coupled system. The control process is easily affected by many uncertain internal and external factors. This study presents an adaptive fuzzy sliding mode control algorithm for such models. The stability of the control system has been proved by the Lyapunov theory. The sliding mode variable structure controller is effective for nonlinear systems and provides strong robustness for systems. The adaptive fuzzy algorithm solves the influence of uncertainty on the system and overcomes the chattering phenomenon caused by the sliding mode control algorithm. This study presents two fuzzy adaptive sliding mode control methods for a fixed-wing UAV model: the first type is a sliding mode controller that adaptively fuzzies only the switching term and the second is a sliding mode controller that adaptively fuzzies both the unknown function and the switching term. These two control methods were compared with the traditional sliding mode control method for attitude, airspeed, and flight altitude control. Numerical simulation results show that the comprehensive fuzzy adaptive sliding mode control can solve the control problems of the strongly coupled nonlinear fixed-wing UAV model. Furthermore, the system uncertainty caused by a large number of unknown disturbances and unknown parameters can be approximated accurately, and the chattering can be eliminated significantly at the same time. This method has a fast response speed, small steady-state error, and strong robustness. It is recommended for complicated, nonlinear, strongly coupled, and multiple uncertain models, such as the fixed-wing and multiple-rotors UAV model.

In future work, we plan to apply the designed controller to a real fixed-wing UAV. The principle is to input the control algorithm into the STM32 chip and design the related hardware system. At same time, it is also planned to design a ground station software to cooperate the UAV to complete flight missions.

Data Availability

The data used to support the findings of this study are included within the article.

Conflicts of Interest

The authors declare that they have no conflicts of interest.

Acknowledgments

This research was funded by Natural Science Foundation of Inner Mongolia Autonomous Region (2019LH01003 and 2021LHMS01002).

References

[1] Y. Kang and J. K. Hedrick, "Linear tracking for a fixed-wing uav using nonlinear model predictive control," *IEEE Transactions on Control Systems Technology*, vol. 17, no. 5, pp. 1202–1210, 2009.

[2] M. Chodnicki, M. Mazur, M. Nowakowski, and G. Kowaleczko, "The mathematical model of uav vertical take-off and landing," *Aircraft Engineering and Aerospace Technology*, vol. 91, no. 2, pp. 249–256, 2019.

[3] J Shen, Y Su, Q Liang, and X Zhu, "Calculation and identification of the aerodynamic parameters for small-scaled fixed-wing UAVS," *Sensors (Basel, Switzerland)*, vol. 18, no. 1, 2018.

[4] J. Liu, M. Sheng, R. Lyu, Y. Shi, and J. Li, "Access points in the air: modeling and optimization of fixed-wing uav network," *IEEE Journal on Selected Areas In Communications*, vol. 38, no. 12, pp. 2824–2835, 2020.

[5] J. Tan and S. Guo, "Backstepping control with fixed-time prescribed performance for fixed wing uav under model uncertainties and external disturbances," *International Journal of Control*, pp. 1–18, 2020.

[6] T. Espinoza, A. Dzul, and M. Llama, "Linear and nonlinear controllers applied to fixed-wing uav," *International Journal of Advanced Robotic Systems*, vol. 10, no. 1, 2013.

[7] R. Mebarki, V. Lippiello, and B. Siciliano, "Nonlinear visual control of unmanned aerial vehicles in gps-denied environments," *IEEE Transactions on Robotics*, vol. 31, no. 4, pp. 1004–1017, 2015.

[8] A. C. Satici, H. Poonawala, and M. W. Spong, "Robust optimal control of quadrotor UAVS," *IEEE Access*, vol. 1, pp. 79–93, 2013.

[9] J. S. Chiou, H. K. Tran, and S. T. Peng, "Attitude control of a single tilt tri-rotor uav system: dynamic modeling and each channel's nonlinear controllers design," *Mathematical Problems In Engineering*, vol. 2013, Article ID 275905, 6 pages, 2013.

[10] J. Zhang, J. Yan, and P. Zhang, "Fixed-wing uav formation control design with collision avoidance based on an improved artificial potential field," *IEEE Access*, vol. 6, Article ID 78342, 2018.

[11] X. Chang, L. Rong, K. Chen, and W. Fu, "LSTM-based output-constrained adaptive fault-tolerant control for fixed-wing uav with high dynamic disturbances and actuator faults," *Mathematical Problems In Engineering*, vol. 2021, Article ID 8882312, 18 pages, 2021.

[12] T. Lee, M. Leok, and N. H. McClamroch, "Nonlinear robust tracking control of a quadrotor uav on se(3)," *Asian Journal of Control*, vol. 15, no. 2, pp. 391–408, 2013.

[13] K. Djamel, M. Abdellah, and A. Benallegue, "Attitude optimal backstepping controller based quaternion for a uav," *Mathematical Problems In Engineering*, vol. 2016, Article ID 8573235, 11 pages, 2016.

[14] F. Chen, R. Jiang, K. Zhang, B. Jiang, and G. Tao, "Robust backstepping sliding-mode control and observer-based fault estimation for a quadrotor UAV," *IEEE Transactions on Industrial Electronics*, vol. 63, no. 8, pp. 5044–5056, 2016.

[15] J. F. Gomez and M. Jamshidi, "Fuzzy adaptive control for a UAV," *Journal of Intelligent and Robotic Systems*, vol. 62, no. 2, pp. 271–293, 2011.

[16] W. Zhou, K. Yin, R. Wang, and Y. E. Wang, "Design of attitude control system for uav based on feedback linearization and adaptive control," *Mathematical Problems In Engineering*, vol. 2014, Article ID 492680, 8 pages, 2014.

[17] T. Espinoza, A. E. Dzul, R. Lozano, and P. Parada, "Backstepping - sliding mode controllers applied to a fixed-wing UAV," *Journal of Intelligent and Robotic Systems*, vol. 73, no. 1, pp. 67–79, 2014.

[18] P. Poksawat, L. Wang, and A. Mohamed, "Automatic tuning of attitude control system for fixed-wing unmanned aerial vehicles," *IET Control Theory and Applications*, vol. 10, no. 17, pp. 2233–2242, 2016.

[19] Z. Zheng, Z. Jin, L. Sun, and M. Zhu, "Adaptive sliding mode relative motion control for autonomous carrier landing of fixed-wing unmanned aerial vehicles," *IEEE Access*, vol. 5, pp. 5556–5565, 2017.

[20] H Castañeda, O. S. S. Peña, and J. D. L. Morales, "Extended observer based on adaptive second order sliding mode control for a fixed wing UAV," *ISA Transactions*, vol. 66, pp. 226–232, 2017.

[21] L. Melkou, M. Hamerlain, and A. Rezoug, "Fixed-wing UAV attitude and altitude control via adaptive second-order sliding mode," *Arabian Journal for Science and Engineering*, vol. 43, no. 12, pp. 6837–6848, 2018.

[22] C. Li, J. Shen, S. Zhai, C. Wang, and J. Yang, "Active flow vector flight control using only sjas for a fixed-wing UAV," *IEEE Access*, vol. 6, Article ID 76535, 2018.

[23] P. Poksawat, L. Wang, and A. Mohamed, "Gain scheduled attitude control of fixed-wing uav with automatic controller tuning," *IEEE Transactions on Control Systems Technology*, vol. 26, no. 4, pp. 1192–1203, 2018.

[24] C. Zhang, G. Zhang, and Q. Dong, "Multi-variable finite-time observer-based adaptive-gain sliding mode control for fixed-wing UAV," *IET Control Theory and Applications*, vol. 15, no. 2, pp. 223–247, 2021.

[25] J. Cheng, H. Yan, J. H. Park, and G. Zong, "Output-feedback control for fuzzy singularly perturbed systems: a nonhomogeneous stochastic communication protocol approach," *IEEE Transactions on Cybernetics*, vol. 2021, Article ID 34236985, 12 pages, 2021.

[26] Y. Wang, X. Xie, M. Chadli, S. Xie, and Y. Peng, "Sliding-mode control of fuzzy singularly perturbed descriptor systems," *IEEE Transactions on Fuzzy Systems*, vol. 29, no. 8, pp. 2349–2360, 2021.

[27] W. Qi, X. Gao, C. K. Ahn, J. Cao, and J. Cheng, "Fuzzy integral sliding-mode control for nonlinear semi-markovian switching systems with application," *IEEE Transactions on Systems, Man, and Cybernetics: Systems*, pp. 1–10, 2020.

[28] W. Qi, J. H. Park, G. Zong, J. Cao, and J. Cheng, "Filter for positive stochastic nonlinear switching systems with phase-type semi-markov parameters and application," *IEEE Transactions on Systems, Man, and Cybernetics: Systems*, pp. 1–12, 2021.

[29] S. Wang, Z. Zhen, J. Jiang, and X. Wang, "Flight tests of autopilot integrated with fault-tolerant control of a small fixed-wing UAV," *Mathematical Problems In Engineering*, vol. 2016, Article ID 2141482, 7 pages, 2016.

[30] L. R. Salinas, E. Slawiñski, and V. A. Mut, "Kinematic nonlinear controller for a miniature helicopter via lyapunov techniques," *Asian Journal of Control*, vol. 16, no. 3, pp. 856–870, 2014.

[31] Y. Mitikiri and K. Mohseni, "Globally stable attitude control of a fixed-wing rudderless uav using subspace projection," *IEEE Robotics and Automation Letters*, vol. 4, no. 2, pp. 1395–1401, 2019.

[32] Y. Han, P. Li, and Z. Zheng, "A non-decoupled backstepping control for fixed-wing UAVs with multivariable fixed-time sliding mode disturbance observer," *Transactions of the Institute of Measurement and Control*, vol. 41, no. 4, pp. 963–974, 2019.

[33] Z. Ali, D. Wang, and M. Aamir, "Fuzzy-based hybrid control algorithm for the stabilization of a tri-rotor UAV," *Sensors*, vol. 16, no. 5, 2016.